AGU ADVANCING EARTH AND SPACE SCIENCES

Geochemistry, Geophysics, Geosystems®

RESEARCH ARTICLE
10.1029/2024GC011444

Key Points:

- During Neo-Tethyan subduction, pyroxenite-bearing domains formed by melt intrusion into the lower lithosphere beneath Eastern Anatolia
- The pyroxenite-bearing domains resulted in gravitational instabilities and led to the foundering of the lithosphere in the Late Miocene
- The regional post-collisional volcanics represent the melts derived both from asthenospheric and delaminated lithospheric mantle domains

Supporting Information:

Supporting Information may be found in the online version of this article.

Correspondence to:

A. Aktağ,
aaktag@munzur.edu.tr

Citation:

Aktağ, A., Sayit, K., Furman, T., & Peters, B. J. (2024). Delamination magmatism in Eastern Anatolia: A geochemical perspective. *Geochemistry, Geophysics, Geosystems*, *25*, e2024GC011444. https://doi.org/10.1029/2024GC011444

Received 9 JAN 2024
Accepted 25 APR 2024

Delamination Magmatism in Eastern Anatolia: A Geochemical Perspective

Alican Aktağ[1,2], Kaan Sayit[1], Tanya Furman[3], and Bradley J. Peters[4]

[1]Department of Geological Engineering, Middle East Technical University, Ankara, Turkey, [2]Rare Earth Elements Application and Research Center, Munzur University, Tunceli, Turkey, [3]Department of Geosciences, Pennsylvania State University, University Park, State College, PA, USA, [4]Institute of Geochemistry and Petrology, ETH Zürich, Zürich, Switzerland

Abstract The Sr-Nd-Hf-Pb isotope geochemistry of the Late Miocene Tunceli Volcanics suggests that they are the products of mixed asthenospheric and lithospheric mantle melts. The combined elemental and mineral chemistry data additionally indicate that a pyroxenite component of lithospheric origin is involved in their genesis. Calculations favor melting depths of ∼2 GPa for the Tunceli lavas, that is, deeper than the current lithosphere-asthenosphere boundary beneath Eastern Anatolia. Geochemical data suggest that during regional Neo-Tethyan subduction, dense (i.e., pyroxenite-bearing) domains formed by progressive melt intrusion into the lower lithosphere resulted in gravitational instabilities. This unstable density configuration eventually led to the foundering of the eastern Anatolian lithosphere in the Late Miocene, resulting in progressive melting of fusible pyroxenite-bearing domains at asthenospheric depths. We demonstrate that these pyroxenitic melts mixed with ambient asthenospheric melts and generated the Tunceli lavas.

Plain Language Summary The Eastern Anatolian High Plateau (EAHP) that formed after the collision of Arabian and Eurasian continents hosts a huge volcanic system. The nature of the source region from which these volcanics originated and the geological dynamics that triggered this widespread volcanic activity are still under debate. We suggest that volcanism occurred when the lithospheric mantle beneath the EAHP separated physically from the overlying crust and sank into the deep asthenosphere. In this study, we explore the geochemical evidence for this model by focusing on the Late Miocene Tunceli Volcanics, one of the early stage members of post-collisional volcanics in the EAHP. Our data suggest that the Tunceli Volcanics are the products of mixed asthenospheric and lithospheric mantle melts. The lithosphere contains a dense pyroxenite component that forms when silica-rich melt invades the lower lithosphere during the subduction process. Calculations have shown that these dense materials melted at higher depths than the base of the lithosphere beneath the region. Thus, we propose that the dense domains in the lower lithosphere resulted in gravitational instabilities and eventually led to the foundering of the eastern Anatolian lithosphere in the Late Miocene.

1. Introduction

The Eastern Anatolian High Plateau (EAHP), with elevations ∼2 km, was formed by the collision of the Eurasian and Arabian continents (Şengör & Yilmaz, 1981). The EAHP is situated between two Neo-Tethyan suture zones and hosts a volumetrically extensive and classic example of post-collisional volcanism (Figure 1; Keskin, 2007). A notable portion of this volcanism emerged between the Late Miocene (∼11 Ma) and Holocene (Keskin, 2007), long after the consumption of the last oceanic realm between the Eurasian and Arabian plates during the Early Miocene (Okay et al., 2010).

The geochemically most primitive mafic lavas (with MgO > 6% wt.) of the EAHP record chemical signatures from their mantle sources. There is a consensus that the post-collisional eastern Anatolian volcanics (PCEAV) are the products of mantle sources containing enriched components (e.g., Aktağ et al., 2022; Özdemir et al., 2022). The debate as to whether lithospheric or asthenospheric mantle has chiefly contributed to PCEAV, the composition and provenance of contributing mantle domains, and the melting depth(s) of this widespread volcanism, however, is still continuing (e.g., Aktağ et al., 2022; Özdemir et al., 2022). Thus, the understanding of the geodynamic evolution of Eastern Anatolia has remained unclear. In this regard, various geodynamic models including adiabatic decompression melting associated with local extension (e.g., Yilmaz et al., 1987), lithospheric delamination (e.g., Pearce et al., 1990), and slab break-off (e.g., Keskin, 2003; Şengör et al., 2003) have been

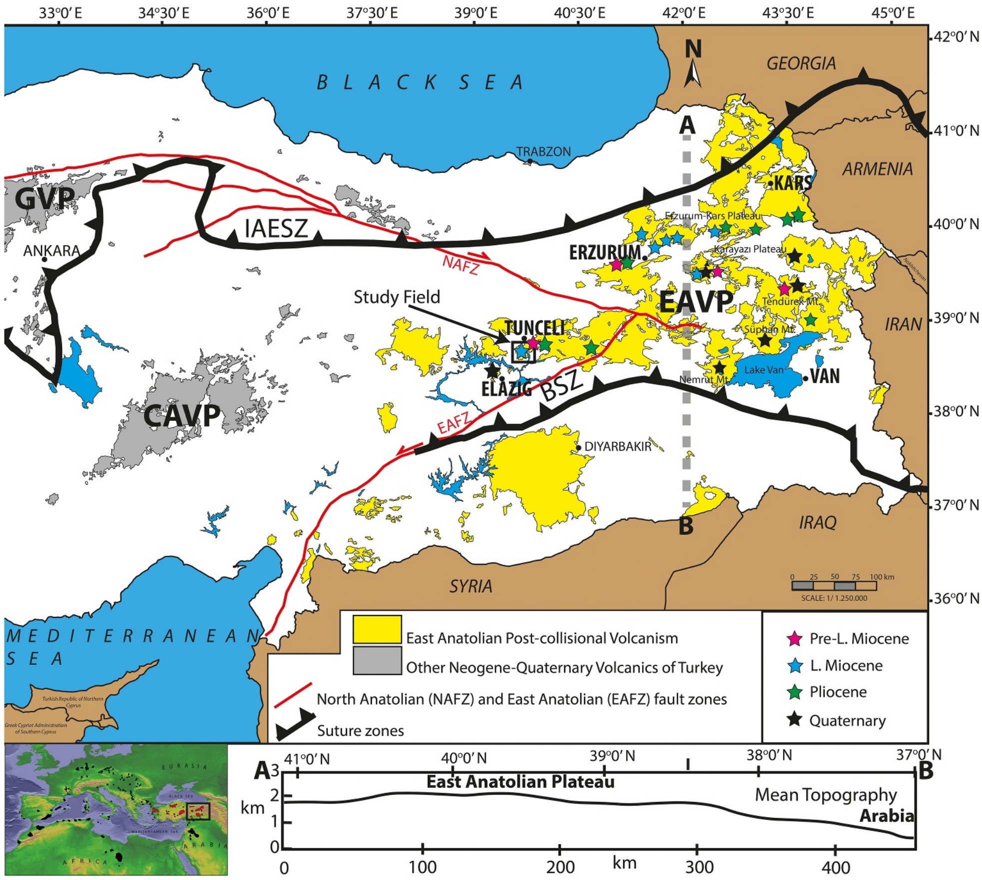

Figure 1. Distribution of eastern Anatolian post-collisional volcanism (simplified from Türkecan, 2015). GVP: Galatian Volcanic Province; CAVP: Central Anatolian Volcanic Province; EAVP: Eastern Anatolian Volcanic Province; IAESZ: Izmir-Ankara-Erzincan Suture Zone; BSZ: Bitlis Suture Zone. Age data are chiefly from the compilation of Kaygusuz et al. (2018) (all references therein). Age data from Tunceli-Elazığ and Karayazı Plateau regions are from Di Giuseppe et al. (2017) and Özdemir et al. (2022), respectively. The N–S topographic profile of the region is from Memiş et al. (2020). The inset digital elevation map (DEM) of the circum-Mediterranean region showing the distribution of the Cenozoic anorogenic volcanic provinces is from the National Oceanic and Atmospheric Administration. The locations of the volcanics on this DEM are from Lustrino and Wilson (2007). The red colors in the DEM map represent the Cenozoic volcanic provinces of Turkey.

suggested to explain the thermal anomalies resulting in mantle melting beneath the EAHP. Among these, recent geophysical data (e.g., Angus et al., 2006; Mahatsente et al., 2018; Ozacar et al., 2008; Zor et al., 2003) have increased research interest in lithospheric foundering dynamics (i.e., slab break-off, drip/delamination) as the triggering mechanism of the widespread post-collisional volcanism in Eastern Anatolia (e.g., Göğüş & Psyklywec, 2008a; Keskin, 2003). Parametric modeling by Göğüş and Pysklywec (2008a) and Memiş et al. (2020) have shown that the geomorphological, geological, and geophysical data from the region are consistent with this sort of delamination dynamics.

In this study, we explore the role of delamination melting during the generation of the PCEAV from a geochemical perspective. Our focus is the Late Miocene (11 Ma; Di Giuseppe et al., 2017) Tunceli Volcanics that erupted during the early stages of the regional widespread post-collisional volcanism. We integrate new mineral chemistry and Sr-Nd-Hf-Pb isotope data with published geochemical data from the region to develop an approximation for the endmember characteristics of mantle source(s) and the melting depths of the products of PCEAV. We then evaluate the geochemical evidence for the delamination melts that erupted in EAHP.

2. Methodology and Sample Selection

This study provides new mineral chemistry and Sr-Nd-Hf-Pb isotopic data from Tunceli Volcanics. All analyses in this study have been conducted on the same sample set used by Aktağ et al. (2019), and the present data have been integrated with their available (from Aktağ et al., 2019) whole-rock major and trace element data.

2.1. Mineral Chemistry

Mineral chemistry analyses were conducted on the phenocryst phases present in the Tunceli Volcanics at the Materials Characterization Laboratory, Pennsylvania State University (USA). The chemical compositions of the phenocryst phases present in five representative samples were measured using a CAMECA SX-50 microprobe with an acceleration voltage of 15Kv, a beam current of 30 nA, and an analytical diameter of 2 μm. The mineral chemistry data are available at Aktağ et al. (2024).

2.2. Sr-Nd-Hf-Pb Isotope Analyses

The freshest 15 basaltic samples from Tunceli Volcanics were selected for Sr-Nd-Hf-Pb isotope analyses based on their petrographical features and whole rock major and trace element geochemistry (see Aktağ et al., 2019). While the Sr and Nd isotope ratios were measured at the Radiogenic Isotope Laboratory, Middle East Technical University (METU), Ankara, Turkey, the Hf, and Pb isotope ratios were determined at the Institute of Geochemistry and Petrology, ETH Zürich, Zürich, Switzerland.

All samples were initially pulverized at METU prior to chromatography and analysis. For Sr and Nd isotope analyses, 100 mg powders of each sample were leached using 4 ml HF (52%) on a hot plate (>100°C) for four days. Samples were dried after leaching and then dissolved on a hot plate using 4 ml 6 N HCL. Following this, the samples were dried again and dissolved in 2.5 N HCL for chromatography. In the first step of chromatography, Sr and Rare Earth Elements (REE) were separated from the matrix using Teflon columns including 2 ml BioRad AG50-W-X8 (100–200 mesh). Afterward, Sr was eluted in 2.5 N HCl before eluting excess Ba in 2.5 N HNO_3. Following these steps, the REE, including Nd, were eluted in 6 N HCl. Finally, Nd was separated from other REE using Teflon columns including 2 ml HDEHP-coated BioRad resin in 0.22 N HCl. After chromatography was finished, the Sr and Nd were loaded on filaments for measurements. Strontium was loaded on single Re filaments combined with 0.005 N H_3PO_4 and Ta activator, whereas Nd was loaded on double Re filaments with 0.005 N H_3PO_4. Strontium and Nd isotope ratio analyses were performed using a thermal ionization mass spectrometer (TIMS, Thermo-Fisher Triton). After measurements, the $^{87}Sr/^{86}Sr$ isotope ratios were normalized to $^{88}Sr/^{86}Sr = 0.1194$, and $^{143}Nd/^{144}Nd$ ratios were normalized to $^{146}Nd/^{144}Nd = 0.7219$. During the analyses, with no bias corrections, the NBS 987 Sr and the LaJolla Nd standards were measured as 0.710248 ± 10 ($n = 4$) and 0.511845 ± 5 ($n = 2$), respectively. The uncertainties for each Sr and Nd isotope measurements are at the 2-sigma level. For more details on sample preparation and chromatography for Sr-Nd isotope analyses, see Köksal et al. (2017).

Following Sr-Nd isotope analyses at METU, the remaining powders of 15 samples were sent to the Institute of Geochemistry and Petrology, ETH Zürich (Switzerland) for Pb-Hf isotope analyses. In the first step of the Pb-Hf chromatography, following a method modified from Strelow and Toerien (1966), Pb was separated in dilute mixtures of HBr and HNO_3 using Teflon columns with 150 μL BioRad AG1-X8 anion resin (100–200 mesh). For each sample, the separation procedure was performed twice to ensure complete separation of Pb from matrix elements. Following Pb separation, the eluted matrix elements were prepared for Hf separation by re-equilibration in HCl. Afterward, on a BioRad PolyPrep column containing 2 ml BioRad AG50-X8 cation resin (200–400 mesh), Hf was separated from major elements in 1 M HCl-0.1 M HF following the method of Patchett and Tatsumoto (1980). Finally, using a method modified by Münker et al. (2001), the samples were oxidized with concentrated $HClO_4$ and HCl, and then Hf was purified on Eichrom LN-Spec resin (1.2 ml resin bed, 100–150 mesh). At the final stage of the chromatography, Hf was collected in 6M HCl-0.4M HF after eluting Zr in 2M HCl-0.1 M HF. The measurements of Pb and Hf isotope ratios were performed by Thermo-Fisher Neptune Plus multi-collector inductively coupled plasma mass spectrometry (MC-ICP-MS). By iteratively calculating a per-session $^{205}Tl/^{203}Tl$ ratio, which minimizes the total offset of the $^{206,207,208}Pb/^{204}Pb$ and $^{207,208}Pb/^{206}Pb$ ratios of NBS 981 from the accepted values (Baker et al., 2004; c.f., Rehkämper & Halliday, 1998), the Pb mass bias was corrected using Tl doping. When the measured Tl/Pb ratios reflected unstable Tl-Pb complexation (i.e., Tl/Pb ratios more than 10% removed from the sample mean), the data were rejected. By using the exponential law, the

Table 1
Sr-Nd-Hf-Pb Isotope Compositions of Tunceli Volcanics

Sample	$^{87}Sr/^{86}Sr$	2σ s.e.	$^{143}Nd/^{144}Nd$	2σ s.e.	$^{206}Pb/^{204}Pb$	2σ s.e.	$^{207}Pb/^{204}Pb$	2σ s.e.	$^{208}Pb/^{204}Pb$	2σ s.e.	$^{176}Hf/^{177}Hf$	2σ s.e.
AV2	0.704261	±8	0.512765	±4	18.7552	±2	15.6915	±1	38.8459	±4	0.282976	±2
AV20	0.704419	±8	0.512736	±5	19.0508	±4	15.7003	±4	39.1682	±13	0.282969	±3
AV24	0.704618	±5	0.512695	±3	19.0845	±5	15.6924	±5	39.2169	±16	0.282926	±2
AV33	0.704165	±5	0.512738	±3	19.0743	±2	15.6777	±2	39.2085	±7	0.282967	±2
AV34	0.705040	±6	0.512702	±2	19.0684	±3	15.6935	±3	39.2038	±12	0.282929	±3
AV38	0.704569	±4	0.512681	±2	18.8469	±5	15.6916	±5	38.9959	±18	0.282901	±2
AV40	0.704933	±6	0.512730	±7	18.9760	±6	15.7145	±6	39.1157	±18	0.282941	±2
AV42	0.704577	±8	0.512746	±4	18.9652	±81	15.6937	±99	39.0521	±330	0.282943	±1
AV49	0.704148	±5	0.512791	±4	18.7256	±73	15.6742	±92	38.7803	±304	0.282983	±2
AV59	0.704519	±5	0.512668	±3	18.8566	±4	15.6917	±5	39.0106	±21	0.282903	±3
AV67	0.704447	±9	0.512748	±9	18.9713	±7	15.7077	±8	39.0866	±29	0.282941	±1
AV70	0.704510	±5	0.512693	±6	18.8255	±39	15.6791	±48	38.9353	±161	0.282908	±3
AV72	0.704173	±4	0.512805	±4	18.8959	±23	15.6437	±27	38.9297	±91	0.282979	±3
AV73	0.704258	±5	0.512814	±7	18.9380	±52	15.6508	±62	38.9754	±207	0.282983	±2
AV75	0.704618	±4	0.512678	±5	18.7686	±75	15.6829	±93	38.8828	±311	0.282924	±1
Reference Materials												
BCR2					18.7698	0.0003	15.6306	0.0003	38.7538	0.0008	0.282865	0.000002
BHVO2					18.4210	0.0004	15.5404	0.0004	38.0829	0.0012	0.283102	0.000002

Note. Standard errors (s.e.) refer to the last digits in the isotope results.

mass fractionation of Hf isotopes was corrected assuming $^{179}Hf/^{177}Hf = 0.7325$. Furthermore, on a per-session basis, the sample compositions were normalized to the accepted JMC-475 value of $^{176}Hf/^{177}Hf = 0.28216$ (c.f., Blichert-Toft & Albarède, 1997). Average per-session 2 SD was 0.0013 for $^{206}Pb/^{204}Pb$, 0.0022 for $^{207}Pb/^{204}Pb$, 0.0055 for $^{208}Pb/^{204}Pb$ ($n_{avg} = 22$ per session), and 0.24ε for $^{176}Hf/^{177}Hf$ ($n_{avg} = 33$ per session). Further analyses of NBS 981, treated through column chemistry, gave $^{206}Pb/^{204}Pb = 16.9381 \pm 0.0032$ (2σ; $n = 13$), $^{207}Pb/^{204}Pb = 15.4939 \pm 0.0043$ (2σ; $n = 13$) and $^{208}Pb/^{204}Pb = 36.7090 \pm 0.0141$ (2σ; $n = 13$). The consistency of these results with the acceptable isotope ratios of each standard excludes any isotopic fractionation during chemical separation. The results of USGS reference materials BCR-2 and BHVO-2 are given in the table of isotopic results (Table 1) for further assessment of the accuracy of the analyses.

3. Results

3.1. Mineral Chemistry

The Tunceli Volcanics are basaltic in composition (Figure S1 in Supporting Information S1; Aktağ et al., 2019), and display generally subophitic/aphyric texture with ~5% phenocryst abundance. Olivine (Fo_{59-85}) is the most abundant phenocryst in these lavas with an interphase percentage of about 60%, followed by ~35% clinopyroxene (augite-$Wo_{40-45}En_{33-48}Fs_{9-23}$ and diopside-$Wo_{45-49}En_{38-46}Fs_{8-15}$), and ~5% plagioclase ($An_{32-66}$). The CaO (wt.%), MnO (wt.%), and FeO (wt.%) contents of the olivines range between 0.20–0.42, 0.18–0.50, and 13.82–33.93, respectively.

Geothermobarometric calculations (Putirka, 2008) on equilibrium clinopyroxenes ($Kd(\text{Fe-Mg})^{\text{cpx-liq}} = 0.27 \pm 0.03$; Putirka, 2008), assuming that the bulk compositions represent liquids, yield crystallization temperatures between 1,075 and 1,153°C and crystallization pressures between 4 and 10.2 kbar. Olivine-liquid thermometric calculations (Putirka et al., 2007) for equilibrium olivines ($^{Fe/Mg}K_{Dmin/liq} = 0.30 \pm 0.03$; Roeder and Emslie, 1970) yield crystallization temperatures between 1,287 and 1,295°C at 1 GPa, corresponding to the highest calculated clinopyroxene crystallization pressure.

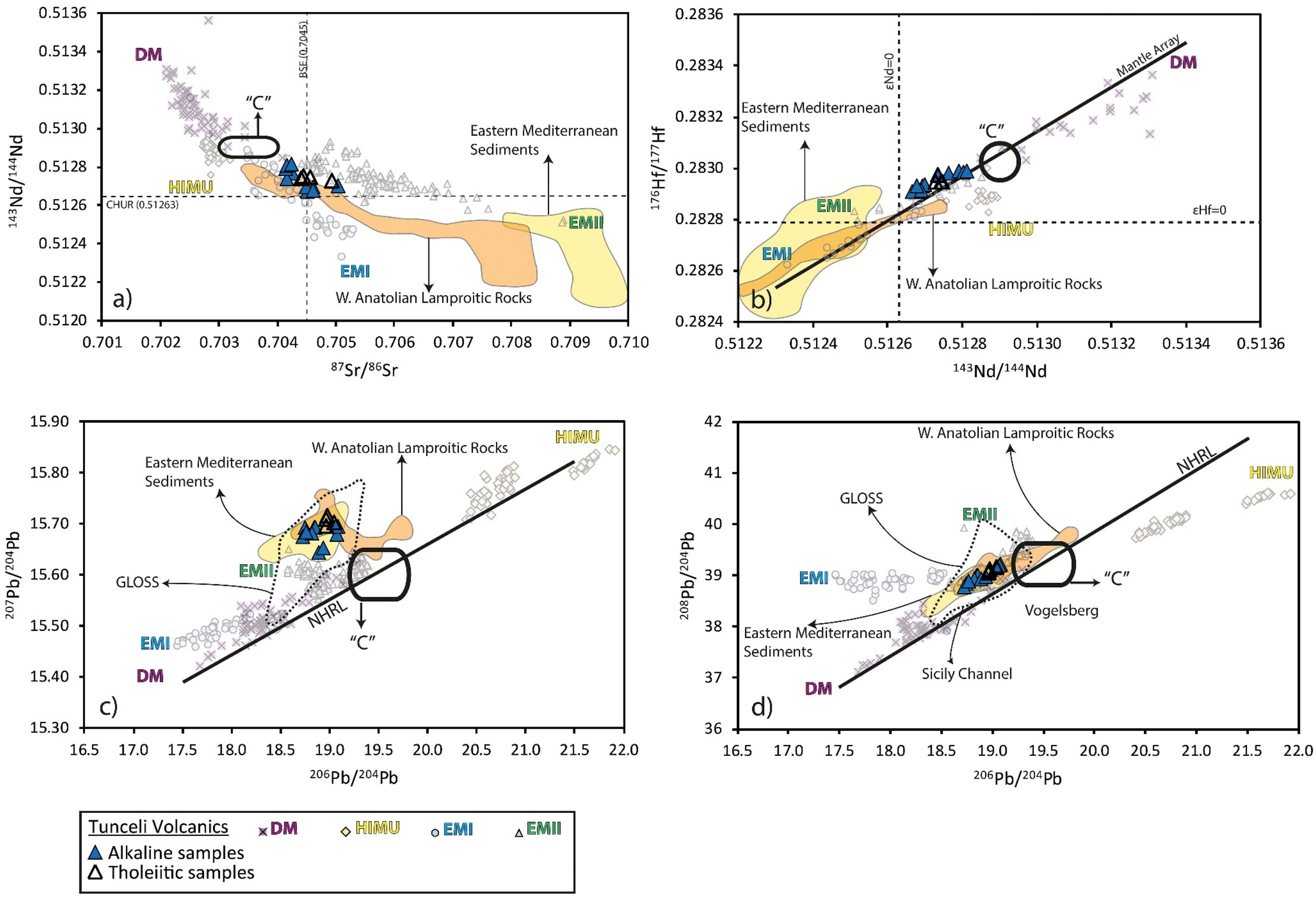

Figure 2. (a) $^{87}Sr/^{86}Sr$ versus $^{143}Nd/^{144}Nd$, (b) $^{143}Nd/^{144}Nd$ versus $^{176}Hf/^{177}Hf$, (c) $^{206}Pb/^{204}Pb$ versus $^{207}Pb/^{204}Pb$ and (d) $^{206}Pb/^{204}Pb$ versus $^{208}Pb/^{204}Pb$ plots for the Tunceli Volcanics. The western Anatolian lamproitic rocks are from Elitok et al. (2010) and Prelević et al. (2012). The eastern Mediterranean sediments are from Klaver et al. (2015). The value of CHUR is from Bouvier et al. (2008) and the Bulk Silicate Earth value is from Salters and Stracke (2004). The mantle array in the plot of $^{143}Nd/^{144}Nd$ versus $^{176}Hf/^{177}Hf$ is from Chauvel et al. (2008). The Sr-Nd-Pb isotope compositions of "C" are from Hanan and Graham (1996). The Hf isotope composition of "C" is from Geldmacher et al. (2011). The NHRL is from Hart (1984). The GLOSS data are from Plank and Langmuir (1998). The data of the MORBs and OIBs are from the compilation of Stracke (2012) and PetDB Database (www.earthchem.org/petdb). The locations of oceanic basalts and their references can be found in the Data Availability Statement.

3.2. Sr-Nd-Hf-Pb Isotope Geochemistry

The Tunceli lavas are subdivided into alkaline and subalkaline (tholeiitic) groups on the basis of their major element geochemistry (Figures S1 and S2 in Supporting Information S1; Aktağ et al., 2019). All samples display unradiogenic to moderately radiogenic $^{87}Sr/^{86}Sr$ (0.704148–0.705040) and unradiogenic $^{143}Nd/^{144}Nd$ (0.512668–0.512814) values. On a plot of $^{87}Sr/^{86}Sr$ versus $^{143}Nd/^{144}Nd$ (Figure 2a), the majority of the samples plot between the global sub-lithospheric mantle component C (Common Component; Hanan & Graham, 1996), assumed to represent recycled oceanic material that has incorporated some continental Pb (Hanan & Graham, 1996) and/or affected by sub-arc alteration (Stracke et al., 2005), and Bulk Silicate Earth, whereas two samples have slightly more radiogenic Sr isotopic compositions and trend toward EMII (Enriched Mantle II; Zindler & Hart, 1986). Their $^{176}Hf/^{177}Hf$ ratios range between 0.282901 and 0.282983, and all samples have Nd-Hf isotopic composition more depleted than the CHondritic Uniform Reservoir (CHUR; Figure 2b). The total data distribution defines a trend between component C and EMII.

The $^{206}Pb/^{204}Pb$, $^{207}Pb/^{204}Pb$, and $^{208}Pb/^{204}Pb$ ratios of the Tunceli lavas range between 18.72–19.08, 15.64–15.71, and 38.78–39.21, respectively. In $^{206}Pb/^{204}Pb$ versus $^{207,208}Pb/^{204}Pb$ (Figures 2c and 2d) diagrams, all samples plot above the Northern Hemisphere Reference Line (NHRL; Hart, 1984) and remain within the field of the Global Subducted Oceanic Sediments (GLOSS; Plank & Langmuir, 1998). In Figure 2c, the lavas exhibit a slightly diffuse cluster above the EMII-type Samoan OIBs, whereas in Figure 2d, they predominantly overlap

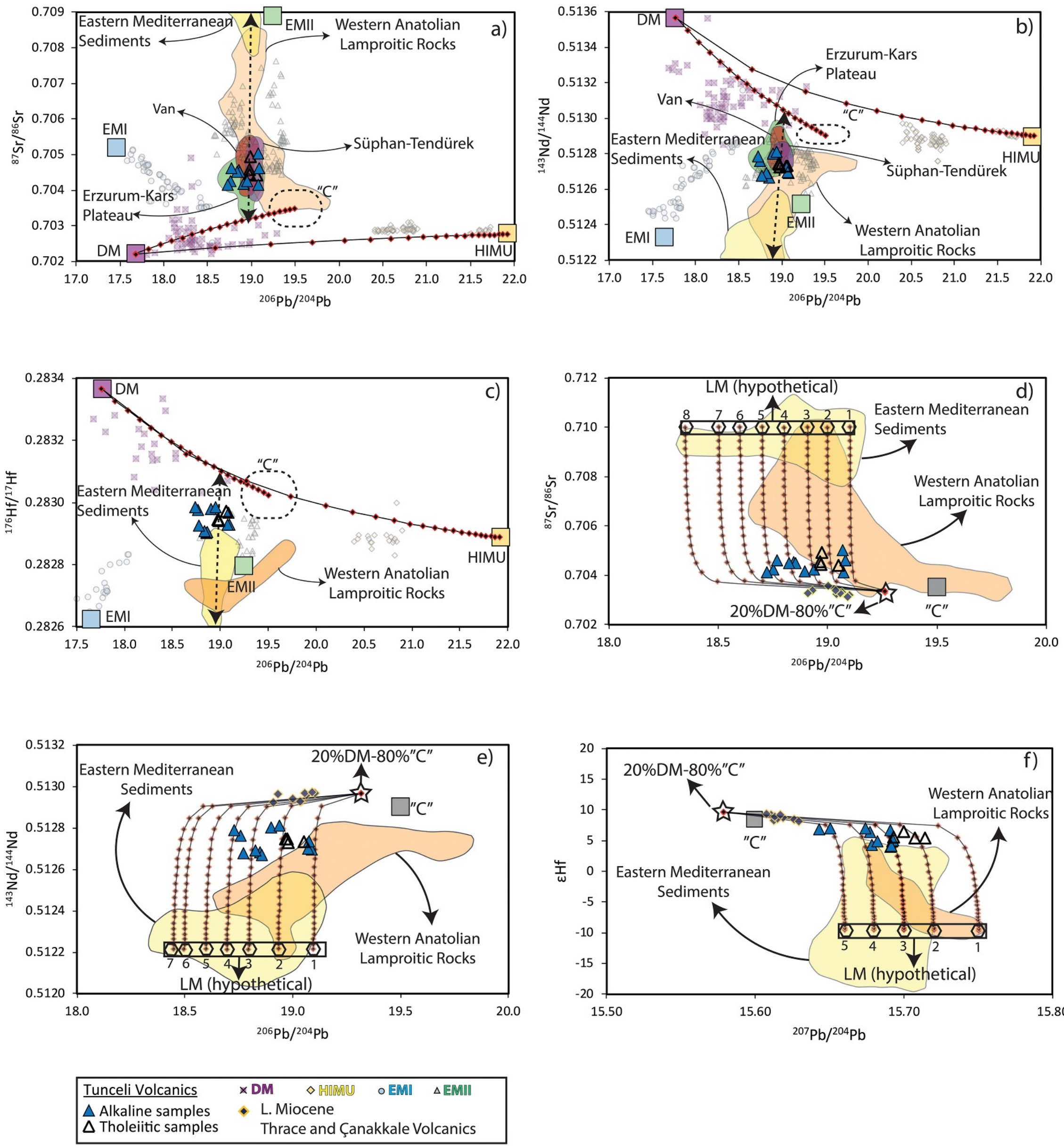

Figure 3. The Sr-Nd-Hf-Pb isotope spaces for Tunceli Volcanics showing calculated solid-state mixing curves between mantle endmembers (a, b, and c), and the melt mixing curves between C-DM (80% C-20% DM) source mixture and lithospheric mantle endmembers (LM) (d, e, and f). The western Anatolian lamproitic rocks are from Elitok et al. (2010) and Prelević et al. (2012). The eastern Mediterranean sediments are from Klaver et al. (2015). The eastern Anatolian lavas with MgO > 4 wt.% are from Oyan et al. (2016, 2017)-Van, Özdemir and Güleç, (2013)-Süphan, Lebedev et al. (2016)-Tendürek, Keskin et al. (2006)-Erzurum-Kars Plateau. The Late Miocene Thrace and Çanakkale lavas with MgO > 4 wt.% are from Aldanmaz et al. (2000, 2006, 2015). For locations and references of the MORBs and OIBs see caption Figure 2. The details of the figure and the modeling parameters can be found in Appendix A.

with the Samoan lavas and define a trend between the DM (Depleted Mantle; Zindler & Hart, 1986) and C components.

4. Discussion

4.1. Mantle Sources

The Sr-Nd-Hf-Pb isotopic systematics of the Tunceli lavas provide several lines of evidence that their mantle source is heterogenous, with the involvement of several distinct components (i.e., C-DM-EMII; Figure 2). In Figures 3a–3c, all Tunceli lavas define a dispersed cluster between a mixture of C and DM and the EMII

10.1029/2024GC011444

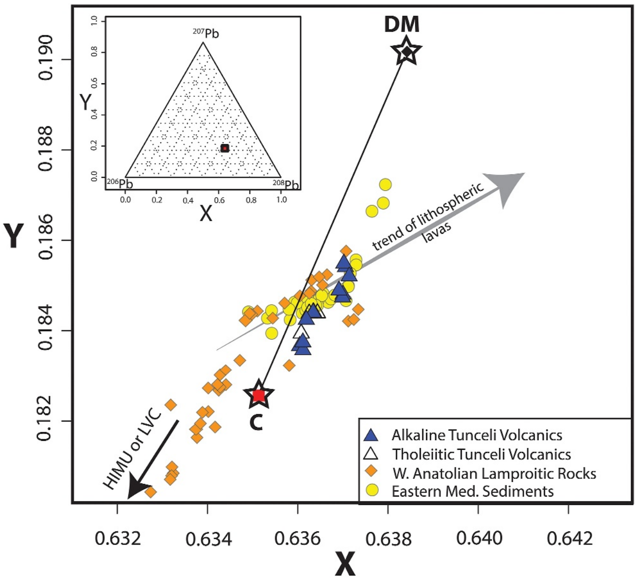

Figure 4. The ternary Pb isotope diagram for the selected Anatolian mafic lavas (after Hanan et al., 1986; Furman et al., 2021). This figure represents the zoomed-in view of the location of the data distribution in the ternary inset. The location of the data is labeled as a red-black square in the ternary inset. The expanded slice of x–y coordinates can also be seen in the ternary inset. The data of the western Anatolian lamproitic rocks are from Elitok et al. (2010); Prelević et al. (2012). The data of eastern Mediterranean sediments are from Klaver et al. (2015). The Pb isotope compositions of "C" are from Hanan and Graham (1996). The Pb isotope compositions were adapted from the most depleted sample from the South Atlantic Ridge (Hanan et al., 1986). HIMU: High μ ($^{238}U/^{204}Pb$) values; Zindler and Hart (1986). LVC: Low-velocity Component; Hoernle et al. (1995).

component and strongly overlap the composition of eastern Anatolian lavas from Van, Süphan-Tendürek, and the Erzurum-Kars plateau. In this multi-component blend, the EMII-like signature does not need to be ancient and deep-seated, such as that tapped by the Samoan lavas (e.g., Jackson et al., 2007), but instead could have been acquired by melt contribution from the modern metasomatized sub-continental lithospheric mantle (SCLM) (e.g., Gall et al., 2021) for two reasons. First, both Tunceli lavas and Anatolian lamproitic rocks (i.e., SCLM-derived melts of Anatolia) share a high $^{207}Pb/^{204}Pb$ ratio at a given $^{206}Pb/^{204}Pb$ ratio compared to many EMII-type Samoan OIBs (Figure 2c), and second, the Tunceli lavas trend toward the compositions of Mediterranean sediments, a potential Tethyan slab-derived agent thought to have fluxed the SCLM beneath eastern Anatolia (Figure 3; see also Aktağ et al., 2022). Alternatively, the EMII-type enrichment in the Pb isotope systematics of the Tunceli lavas can be acquired by melt contribution from the residual metasomatized mantle wedge in the asthenosphere (e.g., Keskin, 2003). This idea, however, appears to be in contrast with the Tunceli lavas since their enriched trace element profile (Figure S3 in Supporting Information S1) together with their Nd-Hf isotope compositions (Figure 2b) argue against derivation from such a highly depleted (e.g., Hochstaedter et al., 2001; Kimura et al., 2016) source region.

The contribution of the SCLM melt into this mixture varies from 5% to 30% according to the melt-mixing modeling (Figures 3d–3f) between a hypothetical heterogeneous lithospheric mantle and an asthenospheric input (C-DM mixture; see Figure 3 caption). This suggests that the asthenospheric input in the genesis of Tunceli lavas is larger (70%–95%) than the SCLM contribution. In addition, a C-dominant (20% DM-80% C) asthenospheric melt contribution is favored based on the calculated curves in Figure 3. The three endmember mixing scenario and the dominance of the C component in this multi-component blend is also apparent in a ternary Pb isotope plot (Figure 4), which is sensitive to distinct source components that have incorporated continent-derived materials (i.e., component C and/or subducted sediments; Hanan & Schilling, 1997; Furman et al., 2021). All Tunceli lavas emerge from the C component and produce a trend oblique to the pseudo-binary mixing line with C and DM. The proximity of the data cluster to the C component indicates a C-dominant mixing dynamics, whereas the deviation of the data trend from the pseudo-binary mixing line between C and DM in the direction of lithospheric mantle melts (i.e., western Anatolian lamproitic rocks) and eastern Mediterranean sediments supports DM and SCLM contributions (Figure 4).

These observations provide compelling evidence that the Tunceli lavas are the products of melt contributions both from lithospheric and asthenospheric mantle regions.

4.2. Pyroxenite Origin

At subduction zones, silica-rich melts from the mantle wedge can intrude into the lower lithosphere and form pyroxenite-bearing domains (with or without garnet, phlogopite, or amphibole) after freezing (e.g., Ducea & Saleeby, 1998; Jull & Kelemen, 2001). The addition of these new phases into the lithosphere increases the local density of the lithosphere and leads to the formation of dense gravitational instabilities (e.g., Jull & Kelemen, 2001; Kay & Kay, 1993; Lee et al., 2006). Based on this hypothesis, the gravitationally unstable lower lithosphere will eventually detach from the main body and sink into the underlying less-dense peridotitic asthenosphere (e.g., Bird, 1979; Houseman et al., 1981). During detachment, the fusible parts of the downgoing lithosphere, especially the pyroxenite-bearing portions (i.e., veins) formed by frozen asthenospheric inputs, are expected to melt first (Elkins-Tanton, 2007). Thus, a lithospheric component with chemical signatures of pyroxenite contributes to volcanism at the early stages of lithospheric foundering events (e.g., Ducea et al., 2013). Accordingly, if regional PCEAV including the Tunceli Volcanics are regarded as the products of such melts, a lithospheric contribution with a pyroxenite signature would be expected in their chemistry.

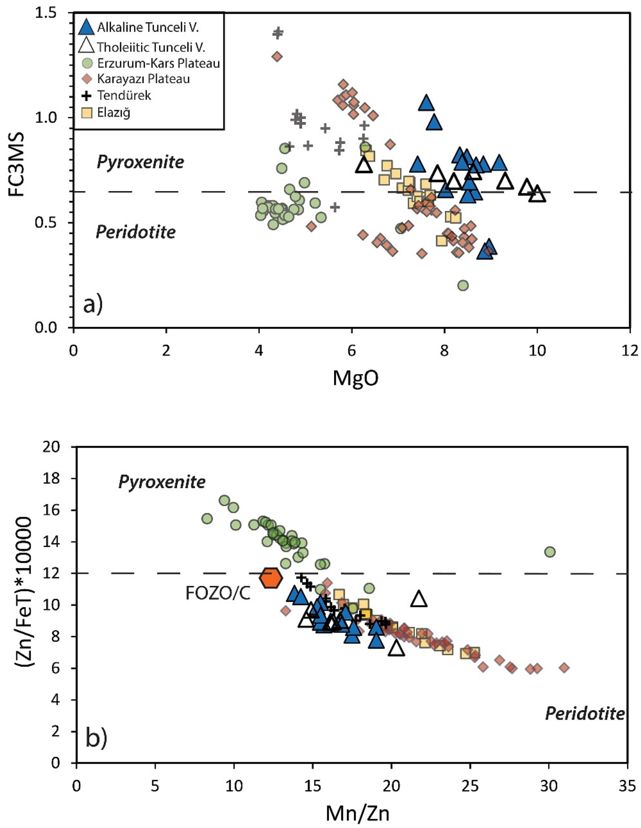

Figure 5. The diagrams of (a) MgO versus FC3MS ($FeO_T/CaO–3MgO/SiO_2$) (wt.%) (Yang & Zhou, 2013) and (b) Mn/Zn versus Zn/Fe (Le Roux et al., 2010, 2011) showing the division line between pyroxenite- and peridotite-derived lavas. The data of the Tunceli lavas (MgO > 6 wt.%) and selected eastern Anatolian lavas (MgO>4 wt.%) are from literature (Aktağ et al., 2019-Tunceli; Keskin et al., 1998-Erzurum Kars Plateau; Özdemir et al., 2022-Karayazı; Lebedev et al., 2016-Tendürek; Aktağ et al., 2022-Elazığ).

Pyroxenite melt contributions can be identified through whole-rock and mineral chemistry of primitive lavas. The FC3MS parameter ($FeO_T/CaO–3MgO/SiO_2$) defined by Yang and Zhou (2013) is useful in distinguishing pyroxenite-derived lavas from peridotite-derived lavas. In this plotting space, the upper limit of FC3MS for peridotitic lavas is 0.65, and larger values are observed in lavas that have a pyroxenite origin. In addition, the Zn/Fe and Zn/Mn ratios in primitive lavas are also regarded as important proxies for the discrimination of lavas derived from peridotite and pyroxenite sources (Le Roux et al., 2010, 2011). It has been postulated that since Zn/Fe and Zn/Mn ratios are difficult to fractionate during peridotite melting but are highly fractionated during pyroxenite melting, high Zn/Fe (i.e., (Zn/FeT) $\times 10^4 > 12$) and Zn/Mn (>0.07) values are expected in lavas derived from a pyroxenite-bearing source (Le Roux et al., 2010, 2011). In addition to these approaches based on whole-rock geochemical data, some studies (e.g., Herzberg, 2011; Sobolev et al., 2005, 2007) have shown that the Ni, Ca, Mn, and Fe contents of olivines in primitive lavas are effective tools in tracing peridotite and pyroxenite melt contributions. Based on this idea, olivines crystallized from a parental magma of a source with pyroxenite are characterized by relatively high Ni and Fe, and low Mn and Ca contents (Herzberg, 2011; Sobolev et al., 2005, 2007).

When Tunceli lavas together with selected PCEAV are plotted on the diagrams of MgO versus FC3MS (Figure 5a), the data distribution of the lavas produces a trend between peridotite and pyroxenite sources (i.e., FC3MS > 0.65) indicating melt contribution both from pyroxenite- and peridotite-bearing source regions. Likewise, the whole-rock (Zn/FeT) $\times 10^4$ values of Tunceli lavas are between 6 and 11, approaching the range of pyroxenite-derived melts (Figure 5b). Tunceli lavas plot within the broad field of the regional PCEAV that extend from lavas with the highest Zn/Fe ratios (i.e., (Zn/FeT) $\times 10^4 > 12$; for example, Erzurum-Kars Plateau lavas), low Mn/Zn ratios to melts with low Zn/Fe (i.e., (Zn/FeT) $\times 10^4 > 12$; for example, Karayazı lavas), and high Mn/Zn ratios, indicating a regionally widespread hybrid source that includes both pyroxenite and peridotite (Figure 5b).

This regional context implies that a pyroxenite component also plays a role in the source of Tunceli lavas. Nevertheless, it should be noted that the elemental geochemical data should be evaluated carefully for the source lithology. Fractional crystallization (FC), which may have been active during the chemical evolution of the lavas, is likely to erase or alter the source fingerprints in the rock chemistry. In this case, since pyroxene mineral phase fractionation would alter the pyroxene-compatible elemental budget of the lavas inherited from their source regions, characterization of pyroxenite source lithology with pyroxene-compatible elements assumes that no possible pyroxene fractionation occurred in the chemical evolution of the lavas. We recognize that the elemental budget of Tunceli volcanism and other PCEAV could have been affected by clinopyroxene fractionation (see Aktağ et al., 2019), so it is possible that the data trends in Figure 5a were created by post-melting processes (the FC3MS parameter contains FC-sensitive elements such as CaO; e.g., Herzberg & Asimov, 2008). However, the high MgO content of Tunceli lavas indicates only a minor role for FC processes and the control of the source lithology on the data trends displayed in Figure 5a is relevant to the genesis of basalts. This interpretation is indeed supported by evaluations (Figure 5b) made by elements (e.g., Zn) that are not compatible with pyroxenes (for basic magmas, $^{cpx\text{-}liq}Zn = 0.5$; Bougault & Hekinian, 1974).

It is important to note that the geochemical signatures observed in Figure 5 can also be observed in lavas derived from convective mantle domains that include recycled lithospheric lithologies (e.g., Herzberg, 2011; Sobolev et al., 2005, 2007). However, as seen in Figure 3, this is not the case for PCEAV, since the Erzurum-Kars lavas with the highest pyroxenite contribution (Figure 5b) do not exhibit obvious C involvement (Figures 3a and 3b). The Pb isotope distribution of Erzurum-Kars lavas (Figures 3a and 3b) indicates that the amount of C involvement

10.1029/2024GC011444

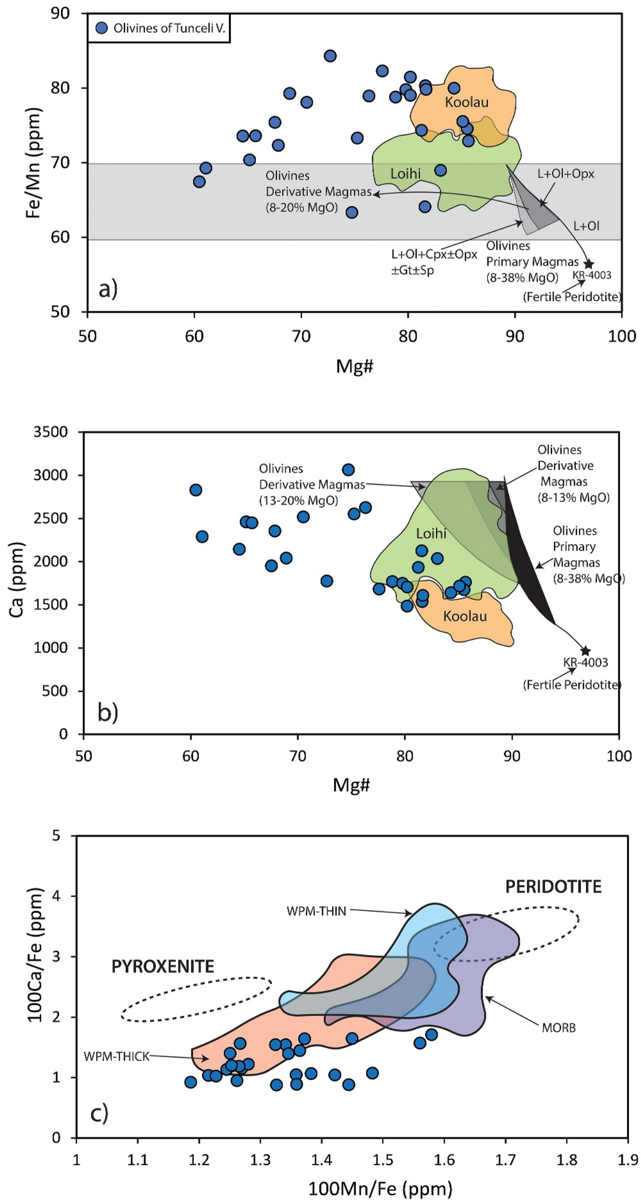

Figure 6. (a) The Mg number versus Fe/Mn (ppm) (Herzberg, 2011), (b) Mg number versus Ca (ppm) (Herzberg, 2011), and 100 Mn/Fe (ppm) versus 100 Ca/Fe (ppm) (Sobolev et al., 2007) diagrams for the olivine compositions of Tunceli Volcanics. The calculated olivine compositions for melts of peridotite sources are from Herzberg (2011) and the olivine compositions for the Hawaiian lavas (Loihi and Koolau Volcanics), WPM-THICK (within plate magmas emplaced over thick lithosphere), WPM-THIN (within plate magmas emplaced over thin lithosphere), and MORB are from Sobolev et al. (2005, 2007).

is the same as that in the genesis of Tunceli lavas (i.e., 20% DM-80% C). Therefore, the pyroxenite imprint in the chemistry of Tunceli lavas and other PCEAV appears to be related to a modern lithospheric origin.

The conclusion above is further supported by the olivine compositions of Tunceli lavas. The majority of the olivines display higher Fe/Mn values and lower Ca content than those which crystallize from melts derived from a purely peridotitic source (Figure 6). Instead, they have Fe, Mn, and Ca contents consistent with olivines of Hawaiian lavas (i.e., Koolau and Loihi; Figures 6a and 6b) and global OIBs emplaced over thick (>70 km) lithosphere (i.e., WPM-THICK: Figure 6c) that are interpreted to have been derived from a hybrid peridotite-pyroxenite source (Figure 6; Herzberg, 2011; Sobolev et al., 2005, 2007). This evidence suggests that the bulk geochemistry of the Tunceli lavas is consistent with the involvement of a pyroxenite component in their genesis.

Phlogopite and amphibole are other potential phases that could have been involved in the source mineralogy of Tunceli lavas as a result of the interaction of slab-released fluid/melt with the peridotite in the base of eastern Anatolian SCLM. We note that the absence of Ba and K anomalies in the trace element systematics of Tunceli lavas precludes the presence of these phases in the source mineralogy of Tunceli Volcanism (see Aktağ et al., 2019 for details). Of note, high-potassium lavas are absent in the whole of Eastern Anatolia; hence, it seems unlikely that the K-bearing phases are involved in the regional mantle underlying the PCEAV. Instead, it is likely that water-poor, low-degree silica-rich melts of sediment column on the downgoing Tethyan slab fluxed the base of eastern Anatolian SCLM and formed fusible pyroxene-bearing domains. It is important to note that mantle pyroxenite xenoliths have been previously reported in Neogene volcanic rocks within the Arabia-Eurasia collision zone and their formation has been attributed to the anhydrous metasomatism of SCLM from the Tethyan slab (Su et al., 2014). The anhydrous (i.e., water-poor) nature of this metasomatic agent is also indicated by the trace element systematics of Tunceli Volcanism. It has been proposed that while Th and light REE (LREE) are transported to the overlying mantle wedge by silicate and/or sediment melts, the fluid-mobile large ion lithophile elements, such as Ba, are prone to transport by aqueous fluids from the top of the subducted slab toward the mantle wedge (Class et al., 2000; Elliott et al., 1997; Pearce & Peate, 1995). The Tunceli lavas display high Th/Yb ratios (0.50–13.90) for a given Ba/La value (5.60–57.40) (Figure S4 in Supporting Information S1). This suggests that the modification of eastern Anatolian SCLM is rather related to slab-derived melts (i.e., silica-rich sediment melt).

4.3. Melting Depth

If the lithospheric mantle delaminates into the asthenosphere due to the gravitational instabilities resulting from the formation of dense fusible pyroxenite-bearing domains at the base of lithosphere, the initial melting zone is expected to be deeper than lithosphere-asthenosphere boundary (LAB) that existed before the foundering event. Accordingly, if delamination magmatism emerged in Eastern Anatolia, the melting region of the delamination magmatics should be much deeper than the current location of the base of the lithosphere beneath the EAHP.

Olivines in Tunceli lavas record very high crystallization temperatures (1,287–1,295°C) that exceed the estimated MORB mantle temperatures (e.g., 1,280°C; McKenzie & Bickle, 1988). This observation suggests that the potential temperatures of melt segregation from the mantle should be higher than these values, which would require

10.1029/2024GC011444

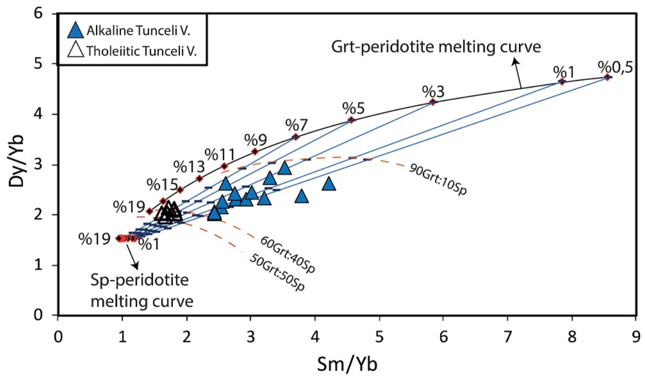

Figure 7. The Sm/Yb versus Dy/Yb melt model for the Tunceli Volcanics (MgO > 6 wt.%). While the source modes and partition coefficients were compiled from McKenzie and O'Nions (1991), melt modes were taken from Thirlwall et al. (1994). The tick marks on each mixing curve correspond to 10% mixing intervals. Gt: Garnet; Sp: Spinel. The source mode, melt mode, and partition coefficients can be found in Table S1 in Supporting Information S1.

higher pressures at melt initiation. To test this idea, we calculated the mantle potential temperatures for the Tunceli lavas using the liquid composition and olivine-liquid equilibration temperatures (Putirka, 2008). The calculated values are between 1,422 and 1,430°C, approximately 120–140°C higher than the calculated olivine crystallization temperatures. This temperature range is consistent with mantle melting at pressures between 2 and 3 GPa under a continent (1,350–1,450°C; Lee et al., 2009). This interpretation is also supported by the calculations of Lee et al. (2009), which yield melt segregation temperatures and pressures for Tunceli lavas between 1,400 and 1,440°C and 1.80–2.24 GPa, respectively (samples with MgO > 8 wt.% and LOI < 1.5 wt.%, and assuming $Fe^{3+}/Fe = 0.1$ and final olivine with Fo_{90}). Based on these calculations, the Tunceli melts appear to have segregated from their mantle source region at depths between 68 and 85 km, assuming the density of the overlying crustal column as 2,700 kg.m^{-3}. Considering that the total thickness of the lithosphere is around ~65 km beneath the Tunceli area (Angus et al., 2006), this scenario corresponds to melt initiation in the asthenosphere, just below the current depth of the lithosphere beneath the region.

Supporting evidence for this depth of melting comes from the REE. Due to the strong partitioning of heavy REE (HREE) into garnet, the LREE/HREE or medium-REE (MREE)/HREE ratios can be useful to trace the presence of garnet in the source (McKenzie & O'Nions, 1991), thereby constraining the depth of melting (Shaw et al., 2003). The REE-based melting modeling of Tunceli lavas (Figure 7) indicates that neither purely spinel-bearing nor purely garnet-bearing source regions are capable of generating the Tunceli lavas; instead, all samples are distributed between the calculated melting curves of spinel- and garnet-peridotite. When considering that the LAB is at ~65 km in the region (Angus et al., 2006) and garnet is assumed to be stable at ~80 km and below (e.g., Takahashi & Kushiro, 1983), the most plausible scenario is to invoke melting in the mantle region where both spinel and garnet phases are stable (i.e., overlapping the spinel-garnet transition zone). This region corresponds to asthenospheric depths of around 80 km and is consistent with the temperature and pressure calculations above. We note that the spinel-bearing source region of Tunceli Volcanism cannot be intrinsic to the lithospheric mantle since the spinel-dominated samples (i.e., tholeiitic; Figure 7) would also display strong SCLM contributions in their geochemistry. As seen in Figure 3, this is not the case for Tunceli lavas. Thus, the melting zone of the Tunceli lavas appears to be deeper than the current location of the LAB, that is, a scenario that can be attributed to a delamination event.

4.4. Regional Geodynamics

Two different mechanisms of lithospheric removal have been envisioned: a brittle (e.g., Bird, 1979) or ductile regime (e.g., Houseman et al., 1981), though a hybrid version is also proposed for some localities (e.g., Stern et al., 2013). These two mechanisms can potentially be distinguished using field and geochemical evidence: (a) the brittle foundering process is assumed to occur in a shorter period than the ductile removal (b) the surface manifestations are axisymmetric in ductile removal compared to brittle removal, and (c) a dominant lithospheric contribution with a stronger pyroxenite chemical signature is expected in lavas derived from a ductile type of removal compared to brittle removal (e.g., Beall et al., 2017; Furman et al., 2016; Göğüş & Pysklywec, 2008b; McMillan & Schoenbohm, 2022; Wang & Currie, 2015).

An asymmetric evolution (i.e., from north to south progression) of volcanism, sedimentary basin formations, uplift, and crustal deformations are well established in Eastern Anatolia (see Memiş et al., 2020). These features suggest that brittle lithospheric removal has chiefly controlled the regional geodynamic evolution of the region since 20 Ma. Our geochemical findings in this study also support the idea that lithospheric removal may be the main triggering mechanism for the generation of PCEAV. However, since the geochemical results require significant involvement of pyroxenite-derived melts in the genesis of PCEAV (up to 30% based on isotopic compositions), we suggest that ductile type of removal via Rayleigh-Taylor instabilities cannot be totally precluded. In other words, a hybrid style of lithospheric foundering, which involves the brittle and ductile types of deformation together, may have been operative in eastern Anatolia. It is important to note that the geochemical data presented in this study are consistent with the removal of the SCLM rather than oceanic slab peel-back beneath the

10.1029/2024GC011444

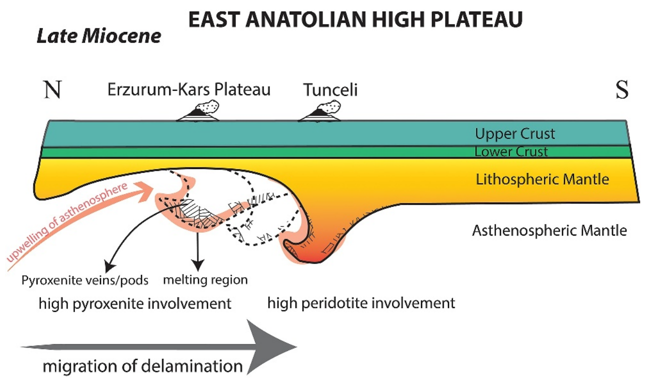

Figure 8. Schematic box model for the delamination magmatism in the East Anatolian High Plateau.

region (see Memiş et al., 2020). The Tethyan oceanic slab (i.e., the southern branch of Neo-Tethys Ocean) steepening and break-off (e.g., Keskin, 2003) process should have occurred before the SCLM detachment beneath the region based on the envisioned geodynamic model.

Since the volcanics in the north of the region (Erzurum-Kars Plateau) are dominated by contributions from a pyroxenite source (Figure 5b), we postulate that the base of the lithosphere in the northern EAHP became denser by silica-rich (with sediment) melt addition through Neo-Tethyan subduction. These solidified melt intrusions (i.e., veins) eventually created gravitational instabilities, resulting in the removal of a part of SCLM beneath the region. In this model, we assume that the delamination involving viscous deformation was triggered beneath the northern EAHP, and then migrated in a short period toward the south (Figure 8). Through the propagation of lithospheric delamination, more sporadic pyroxenite veins intrinsic to the base of the lithosphere in the southern regions should have contributed to the melt generation together with the upwelling asthenospheric mantle (Figure 8). Since a pyroxenite-bearing source has ~150°C lower solidus than average peridotite solidus at upper mantle pressures (Hirschmann & Stolper, 1996), pyroxenite-derived melts are expected to dominate the early stage of the delamination volcanism, whereas peridotite melts would become dominant as the upwelling asthenospheric mantle replaces the foundering portion of lithospheric mantle (Ducea et al., 2013). This model supports the interpretations above and may explain the decrease of pyroxenite and the increase of the peridotitic imprint from north (e.g., Erzurum-Kars Lavas) to south (e.g., Tunceli Lavas).

The removal of SCLM in a ductile-brittle hybrid style provides a geologically reasonable explanation for the surface observations (i.e., geological and morphological; see Memiş et al., 2020) together with the geochemical trends from Eastern Anatolia, and also accounts for the high seismic velocity anomalies (Bakirci et al., 2012; Biryol et al., 2011; Lei & Zhao, 2007; Piromallo & Morelli, 2003; Zor, 2008) in the regional sub-lithospheric mantle.

5. Conclusion

This study presents geochemical evidence that the Late Miocene Tunceli Volcanics are the products of melt mixing involving asthenospheric and lithospheric mantle domains. The lithospheric contributions represent the melting of a pyroxenite-bearing source at greater depths. The results are consistent with the idea that the Tunceli lavas represent melts formed during the early stages of lithospheric delamination, which occurred through a mechanism in which ductile and brittle styles operated together.

Appendix A: Description of Source Mixing (Figures 3a–3c) and Melt Mixing Models (Figures 3d–3f)

Appendix A gives the details of the mixing models used in the article.

A1. Source Mixing

In the source mixing modelings (Figures 3a–3c), the Sr-Nd-Pb isotope compositions of the component "C" are from Hanan and Graham (1996). The Hf composition, on the other hand, was adopted from Geldmacher et al. (2011). In addition, the total isotope range of the component DM was defined according to the most depleted lava among the MORB suite in each diagram. Moreover, regarding the HIMU component, while Sr-Nd isotope compositions were adopted from the sample having the most radiogenic $^{206}Pb/^{204}Pb$ ratio from the Mangaian lava suite, the Hf isotope composition was taken as the average Hf isotope content of the St. Helena lava suite. The references of the data can be found in the Data Availability Statement of the article.

In terms of trace element concentrations, the DM contents were taken from Workman and Hart (2005), whereas those of C and HIMU components were hypothetically calculated from the spreadsheet of Stracke et al. (2003). For C, an ancient oceanic lithosphere that is devoid of its sediment budget (90% depleted lithospheric

10.1029/2024GC011444

Table A1
Isotope and Trace Element Compositions of Mantle Endmembers Used in the Source Mixing Models

	C (Common Comp.)	DM (depleted mantle)	HIMU (High μ)
$^{87}Sr/^{86}Sr$	0.7035	0.702225	0.702791
$^{143}Nd/^{144}Nd$	0.5129	0.513564	0.512899
$^{176}Hf/^{177}Hf$	0.283025	0.283363	0.2828865
$^{206}Pb/^{204}Pb$	19.50	17.681 (Figure 3a)	21.916
		17.762 (Figures 3b and 3c)	
Sr	16.874	7.664	67.014
Nd	1.3839	0.581	8.7196
Hf	0.358	0.157	2.32
Pb	0.299	0.018	0.0929

mantle + 10% oceanic crust) was assumed to melt by 0.5% degree of non-modal accumulated fractional melting at the garnet-stability field. This composition has been chosen since the recycled sediment-free total lithosphere has the potential to display similar isotopic contents with the common component (e.g., PREMA/FOZO/C) in the mantle (Stracke, 2012). For HIMU, on the other hand, only the sediment-free ancient oceanic crust (0% depleted lithospheric mantle + 100% oceanic crust) was assumed to melt in the garnet-stability field. Since such recycled component resembles eclogitic assemblage, the HIMU source was assumed to melt by 4% degree of non-modal accumulated fractional melting. This composition has been chosen since the recycled crust model for the origin of HIMU has been widely accepted by the scientific community (e.g., Hofmann & White, 1982). The sediment cover on the crust has been excluded from the calculation to avoid EM-type enrichment (e.g., Willbold & Stracke, 2006). In the models, while the oceanic lithospheric mantle composition was adopted from Salters and Stracke (2004), the composition of oceanic crust with a package consisting of 25% NMORB + 25% altered MORB + 50% Gabbro was adopted from the calculation of Stracke et al. (2003). The subduction modifications and sediment-melt alterations were allowed in the calculations. The related coefficient values and associated references can be found in the spreadsheet of Stracke et al. (2003). The isotope and trace element contents used in the calculations can be found in the table below (Table A1).

A2. Melt Mixing

For melt mixing modeling between a C-DM mixture and SCLM, the C and DM sources were mixed with each other in different proportions in the first step (e.g., 90%C-10%DM, 80%C-20%DM, 70%C-30%DM, etc.). In these calculations, the isotope and trace element contents of these two sources have been constrained according to the approximation given above. The used values are given in Table A1. Subsequently, each calculated source mixture was assumed to melt by 0.5% degree of nonmodal accumulated fractional melting, and the trace element concentrations (in ppm) of the melts from each source were calculated.

In the second step, lithospheric end-members were constrained based on the literature data. For lithospheric endmember composition, most radiogenic samples among the western Anatolian lamprophyres/lamproites (e.g., Elitok et al., 2010; Prelević et al., 2012), which are attributed to SCLM-derived melts, and eastern Mediterranean sediments (Klaver et al., 2015), which may represent the metasomatic agent modified the SCLM beneath the region, were selected as end-members. Note that, since there are no published data on such lithospheric lithologies in Eastern Anatolia, those of western Anatolian lavas were used. Furthermore, multiple lithospheric endmembers have been used in the modelings to reflect the highly heterogeneous nature of the lithospheric mantle.

In the following step, several melt mixing scenarios were applied between C-DM mixtures and lithospheric mantle endmembers to obtain the most compatible mixing curve for the Tunceli lavas. For this, the Late Miocene Çanakkale-Thrace volcanics (Aldanmaz et al., 2000, 2006, 2015) were also plotted on the diagram to develop a better approximation to the composition of the Anatolian convective mantle. The OIB-like Late Miocene Çanakkale-Thrace lavas are among the C-related Anatolian lavas with the least SCLM contribution in their origin. They are therefore useful for constraining the composition of the C-DM mixture in the genesis of Anatolian lavas. Based on this, the curves constructed between a sub-lithospheric mantle with 80% C component and 20% DM

Table A2
Isotope and Trace Element Compositions of Endmembers Used in the Melt Mixing Models

	Figures	80% C-20% DM	LM1	LM2	LM3	LM4	LM5	LM6	LM7	LM8
$^{87}Sr/^{86}Sr$		0.70337	0.71001							
$^{143}Nd/^{144}Nd$		0.51296	0.512215							
εHf		9.667	−9.512							
$^{206}Pb/^{204}Pb$	3d	19.262	19.10	19.00	18.90	18.80	18.70	18.60	18.50	18.35
	3e	19.32	19.10	18.94	18.80	18.70	18.60	18.50	18.45	-
$^{207}Pb/^{204}Pb$	3f	15.57	15.75	15.72	15.70	15.68	15.66	-	-	-
Sr		846	1,000							
Nd		44.29	74							
Hf		6.95	16.65							
Pb		2.41	241							

component were found to produce the most consistent curves with the Tunceli and Late Miocene Çanakkale-Thrace data. This, indeed, is also supported by the source mixing modelings (Figures 3a–3c), indicating a C-dominant convective mantle for Eastern Anatolia. Based on the results, the sub-lithospheric mantle (80%C-20%DM) and SCLM contributions in the genesis of Tunceli lavas vary between 70%-95% and 5%–30%, respectively.

The isotope and trace element contents used in the melt mixing modelings are given in Table A2. Please note that, as suggested by Hanan et al. (2008), the Pb element concentration (ppm) of SCLM-derived melts was constrained as 100× that of the 80%C-20%DM mixture, and their Sr contents (ppm) were fixed to 1,000 ppm, which is acceptable for most of the lithospheric melts. The Nd and Hf elements of the lithospheric endmembers, on the other hand, were adopted from the sample 05GUE01 by Prelević et al. (2012).

Data Availability Statement

This article is a part of Alican Aktağ's Ph.D. dissertation work (Aktağ, 2022). The mineral chemistry data of Tunceli Volcanics are available at Aktağ et al. (2024). All analyses in this study have been conducted on the same sample set used in Aktağ et al. (2019); the major and trace element data of Tunceli Volcanics can be found in Aktağ et al. (2019). The Anatolian lavas and oceanic basalts (MORBs and OIBs) are also plotted into the diagrams for comparison. The sources of these data are as follows: The data of western Anatolian lamproitic rocks are from Elitok et al. (2010) and Prelević et al. (2012). The data of eastern Mediterranean sediments are from Klaver et al. (2015). The data of Van lavas are available at Oyan et al. (2016, 2017). The data of the Süphan lavas are available at Özdemir and Güleç (2013). The data of Tendürek lavas are available from Lebedev et al. (2016). The data of the Erzurum-Kars Plateau lavas are available at Keskin et al. (1998, 2006). The data of the Late Miocene Thrace and Çanakkale lavas are available at Aldanmaz et al. (2000, 2006, 2015). The data of Karayazı lavas are available at Özdemir et al. (2022). The data of Elazığ lavas are available at Aktağ et al. (2022). The GLOSS (Global Subducted Sediments) data are from Plank and Langmuir (1998). The data of the oceanic basalts (St. Helena and Mangaia Islands: Chaffey et al., 1989; Reisberg et al., 1993; Salters & White, 1998; Salters et al., 2011; Willbold & Stracke, 2006; Woodhead, 1996; South Atlantic Ridge: Agranier et al., 2005; Andres et al., 2004; Cottrell & Kelley, 2013; Fontignie & Schilling, 1996; Hanan et al., 1986; Humphris et al., 1985, Kelley et al., 2013; Pitcairn Island: Eisele et al., 2002; Salters & White, 1998; Woodhead & Devey, 1993; Woodhead & McCulloch, 1989, Samoa Island: Salters et al., 2011; White & Hofmann, 1982, Wright & White, 1987, Workman et al., 2004) are from the compilation of Stracke (2012) and PetDB Database (www.earthchem.org/petdb). Olivine compositions for the Hawaiian (Loihi and Koolau Volcanics), WPM-THICK (within plate magmas emplaced over thick lithosphere), WPM-THIN (within plate magmas emplaced over thin lithosphere), and MORB are from Sobolev et al. (2005, 2007). The data sources for high Th/Yb and high Ba/La arc lavas were obtained from Woodhead et al. (2001) and its compilation (Lesser Antilles: Davidson, 1986; Sunda: Whitford, 1975; Kermadec: Gamble et al., 1993, 1996; Mariana: Gribble et al., 1996; Pearce et al., 1999; Woodhead, 1989; New Britain: Woodhead et al., 1998).

Acknowledgments

This research was supported by METU Scientific Research Project grant (GAP–309–2018–2761 to AA), ETH Zürich/Marie Sklodowska-Curie Actions COFUND (18-1 FEL–28 to BJP), and the Swiss National Science Foundation (PZ00P2 180005 to BJP). We would like to acknowledge S. Bowden and K. Crispin for microprobe analyses at Penn State. We thank S. Köksal for Sr-Nd isotope analyses at METU. We thank Jörg Rickli for his help during isotope analyses at ETH Zürich. We would also like to thank Ö. Karakaş for organizing the Pb-Hf isotope analyses at ETH Zürich. Finally, we are also grateful to Paul D. Asimow for editorial handling, and Cem Yücel and one anonymous reviewer for their constructive and insightful suggestions, which significantly improved the article. This article is a part of Alican Aktağ's Ph.D. dissertation work.

References

Agranier, A., Blichert-Toft, J., Graham, D., Debaille, V., Schiano, P., & Albarède, F. (2005). The spectra of isotopic heterogeneities along the mid-Atlantic Ridge. *Earth and Planetary Science Letters*, *238*(1–2), 96–109. https://doi.org/10.1016/j.epsl.2005.07.011

Aktağ, A. (2022). *Petrogenesis of the Neogene-Quaternary mafic lavas from the Tunceli-Elazığ region (Eastern Turkey)* (PhD Thesis). Middle East Technical University.

Aktağ, A., Önal, A. Ö., & Sayit, K. (2019). Geochemistry of the post-collisional Miocene mafic Tunceli Volcanics, Eastern Turkey: Implications for the nature of the mantle source and melting systematics. *Chemie der Erde*, *79*(1), 113–129. https://doi.org/10.1016/j.geoch.2018.11.004

Aktağ, A., Sayit, K., Furman, T., & Peters, B. J. (2024). Mineral chemistry data of the Tunceli volcanism (eastern Turkey), version 1.0 [Dataset]. *Interdisciplinary Earth Data Alliance (IEDA)*. https://doi.org/10.60520/IEDA/113220

Aktağ, A., Sayit, K., Peters, B. J., Furman, T., & Rickli, J. (2022). Trace element and Sr-Nd-Hf-Pb isotopic constraints on the composition and evolution of eastern Anatolian sub-lithospheric mantle. *Lithos*, *430–431*, 430–431. https://doi.org/10.1016/j.lithos.2022.106849

Aldanmaz, E., Köprübaşi, N., Gürer, Ö. F., Kaymakçi, N., & Gourgaud, A. (2006). Geochemical constraints on the Cenozoic, OIB-type alkaline volcanic rocks of NW Turkey: Implications for mantle sources and melting processes. *Lithos*, *86*(1–2), 50–76. https://doi.org/10.1016/j.lithos.2005.04.003

Aldanmaz, E., Pearce, J. A., Thirlwall, M. F., & Mitchell, J. G. (2000). Petrogenetic evolution of late Cenozoic, post-collision volcanism in western Anatolia, Turkey. *Journal of Volcanology and Geothermal Research*, *102*(1–2), 67–95. https://doi.org/10.1016/S0377-0273(00)00182-7

Aldanmaz, E., Pickard, M., Meisel, T., Altunkaynak, Ş., Sayıt, K., Şen, P., et al. (2015). Source components and magmatic processes in the genesis of Miocene to Quaternary lavas in western Turkey: Constraints from HSE distribution and Hf–Pb–Os isotopes. *Contributions to Mineralogy and Petrology*, *170*(2), 23. https://doi.org/10.1007/s00410-015-1176-x

Andres, M., Blichert-Toft, J., & Schilling, J. G. (2004). Nature of the depleted upper mantle beneath the Atlantic: Evidence from Hf isotopes in normal mid-ocean ridge basalts from 79°N to 55°S. *Earth and Planetary Science Letters*, *225*(1–2), 89–103. https://doi.org/10.1016/j.epsl.2004.05.041

Angus, D. A., Wilson, D. C., Sandvol, E., & Ni, J. F. (2006). Lithospheric structure of the Arabian and Eurasian collision zone in eastern Turkey from S-wave receiver functions. *Geophysical Journal International*, *166*(3), 1335–1346. https://doi.org/10.1111/j.1365-246X.2006.03070.x

Baker, J., Peate, D., Waight, T., & Meyzen, C. (2004). Pb isotopic analysis of standards and samples using a 207Pb-204Pb double spike and thallium to correct for mass bias with a double-focusing MC-ICP-MS. *Chemical Geology*, *211*(3–4), 275–303. https://doi.org/10.1016/j.chemgeo.2004.06.030

Bakirci, T., Yoshizawa, K., & Özer, M. F. (2012). Three-dimensional S-wave structure of the upper mantle beneath Turkey from surface wave tomography. *Geophysical Journal International*, *190*(2), 1058–1076. https://doi.org/10.1111/j.1365-246X.2012.05526.x

Beall, A. P., Moresi, L., & Stern, T. (2017). Dripping or delamination? A range of mechanisms for removing the lower crust or lithosphere. *Geophysical Journal International*, *210*(2), 671–692. https://doi.org/10.1093/gji/ggx202

Bird, P. (1979). Continental delamination and the Colorado Plateau. *Journal of Geophysical Research*, *84*(B13), 7561–7571. https://doi.org/10.1029/JB084iB13p07561

Biryol, C. B., Beck, S. L., Zandt, G., & Özacar, A. A. (2011). Segmented African lithosphere beneath the Anatolian region inferred from teleseismic P-wave tomography. *Geophysical Journal International*, *184*(3), 1037–1057. https://doi.org/10.1111/j.1365-246X.2010.04910.x

Blichert-Toft, J., & Albarède, F. (1997). The Lu-Hf isotope geochemistry of chondrites and the evolution of the mantle-crust system. *Earth and Planetary Science Letters*, *148*(1–2), 243–258. https://doi.org/10.1016/S0012-821X(97)00040-X

Bougault, H., & Hekinian, R. (1974). Rift Valley in the Atlantic Ocean near 36°50′N: Petrology and geochemistry of basaltic rocks. *Earth and Planetary Science Letters*, *24*(2), 249–261. https://doi.org/10.1016/0012-821X(74)90103-4

Bouvier, A., Vervoort, J. D., & Patchett, P. J. (2008). The Lu-Hf and Sm-Nd isotopic composition of CHUR: Constraints from unequilibrated chondrites and implications for the bulk composition of terrestrial planets. *Earth and Planetary Science Letters*, *273*(1–2), 48–57. https://doi.org/10.1016/j.epsl.2008.06.010

Chaffey, D. J., Cliff, R. A., & Wilson, B. M. (1989). *Characterization of the St Helena magma source* (Vol. 42, pp. 257–276). Geological Society Special Publication. https://doi.org/10.1144/GSL.SP.1989.042.01.16

Chauvel, C., Lewin, E., Carpentier, M., Arndt, N. T., & Marini, J. C. (2008). Role of recycled oceanic basalt and sediment in generating the Hf-Nd mantle array. *Nature Geoscience*, *1*(1), 64–67. https://doi.org/10.1038/ngeo.2007.51

Class, C., Miller, D. M., Goldstein, S. L., & Langmuir, C. H. (2000). Distinguishing melt and fluid subduction components in Umnak Volcanics, Aleutian Arc. *Geochemistry, Geophysics, Geosystems*, *1*(6), 1004. https://doi.org/10.1029/1999GC000010

Cottrell, E., & Kelley, K. A. (2013). Redox heterogeneity in mid-ocean ridge basalts as a function of mantle source. *Applied Physics Letters*, *340*(6138), 1314–1317. https://doi.org/10.1063/1.4852615

Davidson, J. P. (1986). Isotopic and trace element constraints on the petrogenesis of subduction-related lavas from Martinique, Lesser Antilles. *Journal of Geophysical Research*, *91*(B6), 5943–5962. https://doi.org/10.1029/JB091iB06p05943

Di Giuseppe, P., Agostini, S., Lustrino, M., Karaoglu, Ö., Savaşçin, M. Y., Manetti, P., & Ersoy, Y. (2017). Transition from compression to strike-slip tectonics revealed by miocene-pleistocene volcanism west of the Karliova triple junction (east Anatolia). *Journal of Petrology*, *58*(10), 2055–2087. https://doi.org/10.1093/petrology/egx082

Ducea, M., & Saleeby, J. (1998). A case for delamination of the deep batholithic crust beneath the Sierra Nevada, California. *International Geology Review*, *40*(1), 78–93. https://doi.org/10.1080/00206819809465199

Ducea, M. N., Seclaman, A. C., Murray, K. E., Jianu, D., & Schoenbohm, L. M. (2013). Mantle-drip magmatism beneath the Altiplano-Puna plateau, central Andes. *Geology*, *41*(8), 915–918. https://doi.org/10.1130/G34509.1

Eisele, J., Sharma, M., Galer, S. J. G., Blichert-Toft, J., Devey, C. W., & Hofmann, A. W. (2002). The role of sediment recycling in EM-1 inferred from Os, Pb, Hf, Nd, Sr isotope and trace element systematics of the Pitcairn hotspot. *Earth and Planetary Science Letters*, *196*(3–4), 197–212. https://doi.org/10.1016/S0012-821X(01)00601-X

Elitok, Ö., Özgür, N., Drüppel, K., Dilek, Y., Platevoet, B., Guillou, H., et al. (2010). Origin and geodynamic evolution of late Cenozoic potassium-rich volcanism in the Isparta area, southwestern Turkey. *International Geology Review*, *52*(4–6), 454–504. https://doi.org/10.1080/00206810902951411

Elkins-Tanton, L. T. (2007). Continental magmatism, volatile recycling, and a heterogeneous mantle caused by lithospheric gravitational instabilities. *Journal of Geophysical Research*, *112*(B3), B03405. https://doi.org/10.1029/2005JB004072

Elliott, T., Plank, T., Zindler, A., White, W., & Bourdon, B. (1997). Element transport from slab to volcanic front at the Mariana arc. *Journal of Geophysical Research*, *102*(B7), 14991–15019. https://doi.org/10.1029/97JB00788

Fontignie, D., & Schilling, J. G. (1996). Mantle heterogeneities beneath the South Atlantic: A Nd-Sr-Pb isotope study along the Mid-Atlantic Ridge (3°S–46°S). *Earth and Planetary Science Letters*, *142*(1–2), 209–221. https://doi.org/10.1016/0012-821x(96)00079-9

Furman, T., Hanan, B. B., Pickard Sjoblom, M., Kürkcüoğlu, B., Sayit, K., Şen, E., et al. (2021). Evolution of mafic lavas in Central Anatolia: Mantle source domains. *Geosphere*, *17*(6), 1631–1646. https://doi.org/10.1130/GES02329.1

Furman, T., Nelson, W. R., & Elkins-Tanton, L. T. (2016). Evolution of the East African rift: Drip magmatism, lithospheric thinning and mafic volcanism. *Geochimica et Cosmochimica Acta*, *185*, 418–434. https://doi.org/10.1016/j.gca.2016.03.024

Gall, H., Furman, T., Hanan, B., Kürkcüoğlu, B., Sayıt, K., Yürür, T., et al. (2021). Post-delamination magmatism in south-central Anatolia. *Lithos*, *398–399*, 106299. https://doi.org/10.1016/j.lithos.2021.106299

Gamble, J., Woodhead, J. O. N., Wright, I. A. N., & Smith, I. A. N. (1996). Basalt and sediment geochemistry and magma petrogenesis in a transect from oceanic island arc to rifted continental margin arc: The Kermadec—Hikurangi Margin, SW Pacific. *Journal of Petrology*, *37*(6), 1523–1546. https://doi.org/10.1093/petrology/37.6.1523

Gamble, J. A., Smith, I. E. M., McCulloch, M. T., Graham, I. J., & Kokelaar, B. P. (1993). The geochemistry and petrogenesis of basalts from the Taupo Volcanic Zone and Kermadec Island Arc, S.W. Pacific. *Journal of Volcanology and Geothermal Research*, *54*(3), 265–290. https://doi.org/10.1016/0377-0273(93)90067-2

Geldmacher, J., Hoernle, K., Hanan, B. B., Blichert-Toft, J., Hauff, F., Gill, J. B., & Schmincke, H. (2011). Hafnium isotopic variations in East Atlantic intraplate volcanism. *Contributions to Mineralogy and Petrology*, *162*(1), 21–36. https://doi.org/10.1007/s00410-010-0580-5

Göğüş, O. H., & Psyklywec, R. N. (2008a). Mantle lithosphere delamination driving plateau uplift and synconvergent extension in eastern Anatolia. *Geology*, *36*(9), 723–726. https://doi.org/10.1130/G24982A.1

Göğüş, O. H., & Pysklywec, R. N. (2008b). Near-surface diagnostics of dripping or delaminating lithosphere. *Journal of Geophysical Research*, *113*(11). https://doi.org/10.1029/2007JB005123

Gribble, R. F., Stern, R. J., Bloomer, S. H., Stüben, D., O'Hearn, T., & Newman, S. (1996). MORB mantle and subduction components interact to generate basalts in the southern Mariana Trough back-arc basin. *Geochimica et Cosmochimica Acta*, *60*(12), 2153–2166. https://doi.org/10.1016/0016-7037(96)00078-6

Hanan, B. B., & Graham, D. W. (1996). Lead and helium isotope evidence from oceanic basalts for a common deep source of mantle plumes. *Science*, *272*(5264), 991–995. https://doi.org/10.1126/science.272.5264.991

Hanan, B. B., Kingsley, R. H., & Schilling, J. G. (1986). Pb isotope evidence in the South Atlantic for migrating ridge – Hotspot interactions. *Nature*, *322*(6075), 137–144. https://doi.org/10.1038/322137a0

Hanan, B. B., & Schilling, J. G. (1997). The dynamic evolution of the Iceland mantle plume: The lead isotope perspective. *Earth and Planetary Science Letters*, *151*(1–2), 43–60. https://doi.org/10.1016/s0012-821x(97)00105-2

Hanan, B. B., Shervais, J. W., & Vetter, S. K. (2008). Yellowstone plume-continental lithosphere interaction beneath the Snake River Plain. *Geology*, *36*(1), 51–54. https://doi.org/10.1130/G23935A.1

Hart, S. R. (1984). A large-scale isotope anomaly in the Southern Hemisphere mantle. *Nature*, *309*(5971), 753–757. https://doi.org/10.1038/309753a0

Herzberg, C. (2011). Identification of source lithology in the Hawaiian and Canary Islands: Implications for origins. *Journal of Petrology*, *52*(1), 113–146. https://doi.org/10.1093/petrology/egq075

Herzberg, C., & Asimow, P. D. (2008). Petrology of some oceanic island basalts: PRIMELT2.XLS software for primary magma calculation. *Geochemistry, Geophysics, Geosystems*, *9*(9). https://doi.org/10.1029/2008GC002057

Hirschmann, M. M., & Stolper, E. M. (1996). A possible role for garnet pyroxenite in the origin of the "garnet signature" in MORB. *Contributions to Mineralogy and Petrology*, *124*(2), 185–208. https://doi.org/10.1007/s004100050184

Hochstaedter, A., Gill, J., Peters, R., Broughton, P., Holden, P., & Taylor, B. (2001). Across-arc geochemical trends in the Izu-Bonin arc: Contributions from the subducting slab. *Geochemistry, Geophysics, Geosystems*, *2*(7). https://doi.org/10.1029/2000GC000105

Hoernle, K., Zhang, Y.-S., & Graham, D. (1995). Seismic and geochemical evidence for large-scale mantle upwelling beneath the eastern Atlantic and western and central Europe. *Nature*, *374*(6517), 34–39. https://doi.org/10.1038/374034a0

Hofmann, A. W., & White, W. M. (1982). Mantle plumes from ancient oceanic crust. *Earth and Planetary Science Letters*, *57*(2), 421–436. https://doi.org/10.1016/0012-821X(82)90161-3

Houseman, G. A., McKenzie, D. P., & Molnar, P. (1981). Convective instability of a thickened boundary layer and its relevance for the thermal evolution of continental convergent belts. *Journal of Geophysical Research*, *86*(B7), 6115–6132. https://doi.org/10.1029/JB086iB07p06115

Humphris, S. E., Thompson, G., Schilling, J.-G., & Kingsley, R. H. (1985). Petrological and geochemical variations along the Mid-Atlantic Ridge between 46°S and 32°S: Influence of the Tristan da Cunha mantle plume. *Geochimica et Cosmochimica Acta*, *49*(6), 1445–1464. https://doi.org/10.1016/0016-7037(85)90294-7

Jackson, M. G., Hart, S. R., Koppers, A. A. P., Staudigel, H., Konter, J., Blusztajn, J., et al. (2007). The return of subducted continental crust in Samoan lavas. *Nature*, *448*(7154), 684–687. https://doi.org/10.1038/nature06048

Jull, M., & Kelemen, P. B. (2001). On the conditions for lower crustal convective instability. *Journal of Geophysical Research*, *106*(B4), 6423–6446. https://doi.org/10.1029/2000jb900357

Kay, R. W., & Kay, S. M. (1993). Delamination and delamination magmatism. *Tectonophysics*, *219*(1), 177–189. https://doi.org/10.1016/0040-1951(93)90295-U

Kaygusuz, A., Aslan, Z., Aydınçakır, E., Yücel, C., Gücer, M. A., & Şen, C. (2018). Geochemical and Sr-Nd-Pb isotope characteristics of the Miocene to Pliocene volcanic rocks from the Kandilli (Erzurum) area, Eastern Anatolia (Turkey): Implications for magma evolution in extension-related origin. *Lithos*, *296–299*, 332–351. https://doi.org/10.1016/j.lithos.2017.11.003

Kelley, K. A., Kingsley, R., & Schilling, J. (2013). Composition of plume-influenced mid-ocean ridge lavas and glasses from the Mid-Atlantic Ridge, East Pacific Rise, Galápagos Spreading Center, and Gulf of Aden. *Geochemistry, Geophysics, Geosystems*, *14*(1), 223–242. https://doi.org/10.1002/ggge.20049

Keskin, M. (2003). Magma generation by slab steepening and breakoff beneath a subduction-accretion complex: An alternative model for collision-related volcanism in Eastern Anatolia, Turkey. *Geophysical Research Letters*, *30*(24), 7–10. https://doi.org/10.1029/2003GL018019

Keskin, M. (2007). *Eastern Anatolia: A hotspot in a collision zone without a mantle plume* (Vol. 430, pp. 693–722). Special Paper of the Geological Society of America. https://doi.org/10.1130/2007.2430(32)

Keskin, M., Pearce, J. A., Kempton, P. D., & Greenwood, P. (2006). Magma-crust interactions and magma plumbing in a postcollisional setting: Geochemical evidence from the Erzurum-Kars volcanic plateau, eastern Turkey. *Special Paper of the Geological Society of America*, *409*(23), 475–505. https://doi.org/10.1130/2006.2409

Keskin, M., Pearce, J. A., & Mitchell, J. G. (1998). Volcano-stratigraphy and geochemistry of collision-related volcanism on the Erzurum-Kars Plateau, northeastern Turkey. *Journal of Volcanology and Geothermal Research*, *85*(1–4), 355–404. https://doi.org/10.1016/S0377-0273(98)00063-8

Kimura, J., Gill, J. B., Skora, S., van Keken, P. E., & Kawabata, H. (2016). Origin of geochemical mantle components: Role of subduction filter. *Geochemistry, Geophysics, Geosystems*, *17*(8), 3289–3325. https://doi.org/10.1002/2016GC006343

Klaver, M., Djuly, T., de Graaf, S., Sakes, A., Wijbrans, J., Davies, G., & Vroon, P. (2015). Temporal and spatial variations in provenance of Eastern Mediterranean Sea sediments: Implications for Aegean and Aeolian arc volcanism. *Geochimica et Cosmochimica Acta*, *153*, 149–168. https://doi.org/10.1016/j.gca.2015.01.007

Köksal, S., Toksoy-Köksal, F., & Göncüoglu, M. C. (2017). Petrogenesis and geodynamics of plagiogranites from Central Turkey (Ekecikdağ/Aksaray): New geochemical and isotopic data for generation in an arc basin system within the northern branch of Neotethys. *International Journal of Earth Sciences*, *106*(4), 1181–1203. https://doi.org/10.1007/s00531-016-1401-5

Lebedev, V. A., Sharkov, E. V., Ünal, E., & Keskin, M. (2016). Late Pleistocene Tendürek Volcano (eastern Anatolia, Turkey): I. Geochronology and petrographic characteristics of igneous rocks. *Петрология*, *24*(2), 142–167. https://doi.org/10.7868/s0869590316020047

Lee, C. T. A., Cheng, X., & Horodyskyj, U. (2006). The development and refinement of continental arcs by primary basaltic magmatism, garnet pyroxenite accumulation, basaltic recharge and delamination: Insights from the Sierra Nevada, California. *Contributions to Mineralogy and Petrology*, *151*(2), 222–242. https://doi.org/10.1007/s00410-005-0056-1

Lee, C. T. A., Luffi, P., Plank, T., Dalton, H., & Leeman, W. P. (2009). Constraints on the depths and temperatures of basaltic magma generation on Earth and other terrestrial planets using new thermobarometers for mafic magmas. *Earth and Planetary Science Letters*, *279*(1–2), 20–33. https://doi.org/10.1016/j.epsl.2008.12.020

Lei, J., & Zhao, D. (2007). Teleseismic evidence for a break-off subducting slab under Eastern Turkey. *Earth and Planetary Science Letters*, *257*(1–2), 14–28. https://doi.org/10.1016/j.epsl.2007.02.011

Le Roux, V., Dasgupta, R., & Lee, C.-T. A. (2011). Mineralogical heterogeneities in the Earth's mantle: Constraints from Mn, Co, Ni and Zn partitioning during partial melting. *Earth and Planetary Science Letters*, *307*(3), 395–408. https://doi.org/10.1016/j.epsl.2011.05.014

Le Roux, V., Lee, C. T. A., & Turner, S. J. (2010). Zn/Fe systematics in mafic and ultramafic systems: Implications for detecting major element heterogeneities in the Earth's mantle. *Geochimica et Cosmochimica Acta*, *74*(9), 2779–2796. https://doi.org/10.1016/j.gca.2010.02.004

Lustrino, M., & Wilson, M. (2007). The circum-Mediterranean anorogenic Cenozoic igneous province. *Earth-Science Reviews*, *81*(1–2), 1–65. https://doi.org/10.1038/nature06688002

Mahatsente, R., Önal, G., & Çemen, I. (2018). Lithospheric structure and the isostatic state of Eastern Anatolia: Insight from gravity data modelling. *Lithosphere*, *10*(2), 279–290. https://doi.org/10.1130/L685.1

Mckenzie, D., & Bickle, M. J. (1988). The volume and composition of melt generated by extension of the lithosphere. *Journal of Petrology*, *29*(3), 625–679. https://doi.org/10.1093/petrology/29.3.625

McKenzie, D., & O'Nions, R. K. (1991). Partial melt distributions from inversion of rare Earth element concentrations. *Journal of Petrology*, *32*(5), 1021–1091. https://doi.org/10.1093/petrology/32.5.1021

McMillan, M., & Schoenbohm, L. M. (2022). Diverse styles of lithospheric dripping: Synthesizing gravitational instability models, continental tectonics, and geologic observations. *Geochemistry, Geophysics, Geosystems*, *24*(2). https://doi.org/10.1029/2022gc010488

Memiş, C., Gö, H., Uluocak, E. Ş., Pysklywec, R., Keskin, M., Şengör, A. C., & Topuz, G. (2020). Long wavelength progressive plateau uplift in eastern anatolia since 20 Ma: Implications for the role of slab peel – Back and break – Off. *Geochemistry, Geophysics, Geosystems*, *21*(2), 1–24. https://doi.org/10.1029/2019GC008726

Münker, C., Weyer, S., Scherer, E., & Mezger, K. (2001). Separation of high field strength elements (Nb, Ta, Zr, Hf) and Lu from rock samples for MC-ICPMS measurements. *Geochemistry, Geophysics, Geosystems*, *2*(12). https://doi.org/10.1029/2001GC000183

Okay, A. I., Zattin, M., & Cavazza, W. (2010). Apatite fission-track data for the Miocene Arabia-Eurasia collision. *Geology*, *38*(1), 35–38. https://doi.org/10.1130/G30234.1

Oyan, V., Keskin, M., Lebedev, V. A., Chugaev, A. V., & Sharkov, E. V. (2016). Magmatic evolution of the Early Pliocene Etrüsk stratovolcano, Eastern Anatolian Collision Zone, Turkey. *Lithos*, *256–257*, 88–108. https://doi.org/10.1016/j.lithos.2016.03.017

Oyan, V., Keskin, M., Lebedev, V. A., Chugaev, A. V., Sharkov, E. V., & Ünal, E. (2017). Petrology and geochemistry of the quaternary mafic volcanism to the NE of Lake Van, Eastern Anatolian collision zone, Turkey. *Journal of Petrology*, *58*(9), 1701–1728. https://doi.org/10.1093/petrology/egx070

Ozacar, A. A., Gilbert, H., & Zandt, G. (2008). Upper mantle discontinuity structure beneath East Anatolian Plateau (Turkey) from receiver functions. *Earth and Planetary Science Letters*, *269*(3–4), 427–435. https://doi.org/10.1016/j.epsl.2008.02.036

Özdemir, Y., & Güleç, N. (2013). Geological and geochemical evolution of the quaternary süphan stratovolcano, Eastern Anatolia, Turkey: Evidence for the lithosphere-asthenosphere interaction in post-collisional volcanism. *Journal of Petrology*, *55*(1), 37–62. https://doi.org/10.1093/petrology/egt060

Özdemir, Y., Oyan, V., & Jourdan, F. (2022). Petrogenesis of Middle Miocene to Early Quaternary basalts from the Karayazı–Göksu plateau (Eastern Anatolia, Turkey): Implication for the role of pyroxenite and lithospheric thickness. *Lithos*, *416–417*, 416–417. https://doi.org/10.1016/j.lithos.2022.106671

Patchett, P. J., & Tatsumoto, M. (1980). Hafnium isotope variations in oceanic basalts. *Geophysical Research Letters*, *7*(12), 1077–1080. https://doi.org/10.1029/GL007i012p01077

Pearce, J. A., Bender, J. F., De Long, S. E., Kidd, W. S. F., Low, P. J., Güner, Y., et al. (1990). Genesis of collision volcanism in Eastern Anatolia, Turkey. *Journal of Volcanology and Geothermal Research*, *44*(1–2), 189–229. https://doi.org/10.1016/0377-0273(90)90018-B

Pearce, J. A., Kempton, P. D., Nowell, G. M., & Noble, S. R. (1999). Hf-Nd element and isotope perspective on the nature and provenance of mantle and subduction components in western Pacific Arc-Basin systems. *Journal of Petrology*, *40*(11), 1579–1611. https://doi.org/10.1093/petroj/40.11.1579

Pearce, J. A., & Peate, D. W. (1995). Tectonic implications of the composition of volcanic ARC magmas. *Annual Review of Earth and Planetary Sciences*, *23*(1), 251–285. https://doi.org/10.1146/annurev.ea.23.050195.001343

Piromallo, C., & Morelli, A. (2003). P wave tomography of the mantle under the Alpine-Mediterranean area. *Journal of Geophysical Research*, *108*(B2). https://doi.org/10.1029/2002jb001757

Plank, T., & Langmuir, C. H. (1998). The chemical composition of subducting sediment and its consequences for the crust and mantle. *Chemical Geology*, *145*(3–4), 325–394. https://doi.org/10.1016/S0009-2541(97)00150-2

Prelević, D., Akal, C., Foley, S. F., Romer, R. L., Stracke, A., & Van den Bogaard, P. (2012). Ultrapotassic mafic rocks as geochemical proxies for post-collisional dynamics of orogenic lithospheric mantle: The case of southwestern Anatolia, Turkey. *Journal of Petrology*, *53*(5), 1019–1055. https://doi.org/10.1093/petrology/egs008

Putirka, K. D. (2008). Thermometers and barometers for volcanic systems. *Reviews in Mineralogy and Geochemistry*, *69*(December), 61–120. https://doi.org/10.2138/rmg.2008.69.3

Putirka, K. D., Perfit, M., Ryerson, F. J., & Jackson, M. G. (2007). Ambient and excess mantle temperatures, olivine thermometry, and active vs. passive upwelling. *Chemical Geology*, *241*(3–4), 177–206. https://doi.org/10.1016/j.chemgeo.2007.01.014

Rehkämper, M., & Halliday, A. N. (1998). Accuracy and long-term reproducibility of lead isotopic measurements by multiple-collector inductively coupled plasma mass spectrometry using an external method for correction of mass discrimination. *International Journal of Mass Spectrometry*, *181*(1–3), 123–133. https://doi.org/10.1016/s1387-3806(98)14170-2

Reisberg, L., Zindler, A., Marcantonio, F., White, W., Wyman, D., & Weaver, B. (1993). Os isotope systematics in ocean island basalts. *Earth and Planetary Science Letters*, *120*(3–4), 149–167. https://doi.org/10.1016/0012-821X(93)90236-3

Roeder, P. L., & Emslie, R. F. (1970). Olivine-liquid equilibrium. *Contributions to Mineralogy and Petrology*, *29*(4), 275–289. https://doi.org/10.1007/BF00371276

Salters, V. J. M., Mallick, S., Hart, S. R., Langmuir, C. E., & Stracke, A. (2011). Domains of depleted mantle: New evidence from hafnium and neodymium isotopes. *Geochemistry, Geophysics, Geosystems*, *12*(8). https://doi.org/10.1029/2011GC003617

Salters, V. J. M., & Stracke, A. (2004). Composition of the depleted mantle. *Geochemistry, Geophysics, Geosystems*, *34*(5). https://doi.org/10.1029/2003GC000597

Salters, V. J. M., & White, W. M. (1998). Hf isotope constraints on mantle evolution. *Chemical Geology*, *145*(3–4), 447–460. https://doi.org/10.1016/S0009-2541(97)00154-X

Şengör, A. M. C., Özeren, S., Genç, T., & Zor, E. (2003). East Anatolian High Plateau as a mantle-supported, north-south shortened domal structure. *Geophysical Research Letters*, *30*(24), 2–5. https://doi.org/10.1029/2003GL017858

Şengör, A. M. C., & Yilmaz, Y. (1981). Tethyan evolution of Turkey: A plate tectonic approach. *Tectonophysics*, *75*(3–4), 181–241. https://doi.org/10.1016/0040-1951(81)90275-4

Shaw, J. E., Baker, J. A., Menzies, M. A., Thirlwall, M. F., & Ibrahim, K. M. (2003). Petrogenesis of the largest intraplate volcanic field on the Arabian plate (Jordan): A mixed lithosphere–asthenosphere source activated by lithospheric extension. *Journal of Petrology*, *44*(9), 1657–1679. https://doi.org/10.1093/petrology/egg052

Sobolev, A. V., Hofmann, A. W., Kuzmin, D. V., Yaxley, G. M., Arndt, N. T., Chung, S.-L., et al. (2007). The amount of recycled crust in sources of mantle-derived melts. *Science*, *316*(5823), 412–417. https://doi.org/10.1126/science.1138113

Sobolev, A. V., Hofmann, A. W., Sobolev, S. V., & Nikogosian, I. K. (2005). An olivine-free mantle source of Hawaiian shield basalts. *Nature*, *434*(7033), 590–597. https://doi.org/10.1038/nature03411

Stern, T., Houseman, G., Salmon, M., & Evans, L. (2013). Instability of a lithospheric step beneath western North Island, New Zealand. *Geology*, *41*(4), 423–426. https://doi.org/10.1130/G34028.1

Stracke, A. (2012). Earth's heterogeneous mantle: A product of convection-driven interaction between crust and mantle. *Chemical Geology*, *330–331*, 274–299. https://doi.org/10.1016/j.chemgeo.2012.08.007

Stracke, A., Bizimis, M., & Salters, V. J. M. (2003). Recycling oceanic crust: Quantitative constraints. *Geochemistry, Geophysics, Geosystems*, *4*(3). https://doi.org/10.1029/2001GC000223

Stracke, A., Hofmann, A. W., & Hart, S. R. (2005). FOZO, HIMU, and the rest of the mantle zoo. *Geochemistry, Geophysics, Geosystems*, *6*(5). https://doi.org/10.1029/2004GC000824

Strelow, F. W. E., & Toerien, F. S. (1966). Separation of Lead(II) from Bismuth(III), Thallium(III), Cadmium(II), Mercury(II), Gold(III), Platinum(IV), Palladium(II), and other elements by anion exchange chromatography. *Analytical Chemistry*, *38*(4), 545–548. https://doi.org/10.1021/ac60236a006

Su, B. X., Chung, S. L., Zarrinkoub, M. H., Pang, K. N., Chen, L., Ji, W. Q., et al. (2014). Composition and structure of the lithospheric mantle beneath NE Iran: Constraints from mantle xenoliths. *Lithos*, *202–203*, 267–282. https://doi.org/10.1016/j.lithos.2014.06.002

Takahashi, E., & Kushiro, I. (1983). Melting of a dry peridotite at high pressures and basalt magma genesis. *American Mineralogist*, *68*(9–10), 859–879.

Thirlwall, M. F., Upton, B. G. J., & Jenkins, C. (1994). Interaction between continental lithosphere and the Iceland plume--Sr-Nd-Pb isotope geochemistry of tertiary basalts, NE Greenland. *Journal of Petrology*, *35*(3), 839–879. https://doi.org/10.1093/petrology/35.3.839

Türkecan, A. (2015). *Türkiye'nin Senozoyik Volkanitleri*. MTA Genel Müdürlüğü Yayınları.

Wang, H., & Currie, C. A. (2015). Magmatic expressions of continental lithosphere removal. *Journal of Geophysical Research: Solid Earth*, *120*(10), 7239–7260. https://doi.org/10.1002/2015JB012112

White, W. M., & Hofmann, A. W. (1982). Sr and Nd isotope geochemistry of oceanic basalts and mantle evolution. *Nature*, *296*(5860), 821–825. https://doi.org/10.1038/296821a0

Whitford, D. J. (1975). *Geochemistry and petrology of volcanic rocks from the Sunda arc, Indonesia* (PhD Thesis (Unpublished)). Australian National University.

Willbold, M., & Stracke, A. (2006). Trace element composition of mantle end-members: Implications for recycling of oceanic and upper and lower continental crust. *Geochemistry, Geophysics, Geosystems*, *7*(4), 1–30. https://doi.org/10.1029/2005GC001005

Woodhead, J. D. (1989). Geochemistry of the Mariana arc (western Pacific): Source composition and processes. *Chemical Geology*, *76*(1), 1–24. https://doi.org/10.1016/0009-2541(89)90124-1

Woodhead, J. D. (1996). Extreme HIMU in an oceanic setting: The geochemistry of Mangaia Island (Polynesia), and temporal evolution of the Cook-Austral hotspot. *Journal of Volcanology and Geothermal Research*, *72*(1–2), 1–19. https://doi.org/10.1016/0377-0273(96)00002-9

Woodhead, J. D., & Devey, C. W. (1993). Geochemistry of the Pitcairn seamounts, I: Source character and temporal trends. *Earth and Planetary Science Letters*, *116*(1–4), 81–99. https://doi.org/10.1016/0012-821X(93)90046-C

Woodhead, J. D., Eggins, S. M., & Johnson, R. W. (1998). Magma genesis in the new Britain Island Arc: Further insights into melting and mass transfer processes. *Journal of Petrology*, *39*(9), 1641–1668. https://doi.org/10.1093/petroj/39.9.1641

Woodhead, J. D., Hergt, J. M., Davidson, J. P., & Eggins, S. M. (2001). Hafnium isotope evidence for 'conservative' element mobility during subduction zone processes. *Earth and Planetary Science Letters*, *192*(3), 331–346. https://doi.org/10.1016/S0012-821X(01)00453-8

Woodhead, J. D., & McCulloch, M. T. (1989). Ancient seafloor signals in Pitcairn Island lavas and evidence for large amplitude, small length-scale mantle heterogeneities. *Earth and Planetary Science Letters*, *94*(3–4), 257–273. https://doi.org/10.1016/0012-821X(89)90145-3

Workman, R. K., & Hart, S. R. (2005). Major and trace element composition of the depleted MORB mantle (DMM). *Earth and Planetary Science Letters*, *231*(1–2), 53–72. https://doi.org/10.1016/j.epsl.2004.12.005

Workman, R. K., Hart, S. R., Jackson, M., Regelous, M., Farley, K. A., Blusztajn, J., et al. (2004). Recycled metasomatized lithosphere as the origin of the Enriched Mantle II (EM2) end-member: Evidence from the Samoan Volcanic Chain. *Geochemistry, Geophysics, Geosystems*, *5*(4), 1–44. https://doi.org/10.1029/2003GC000623

Wright, E., & White, W. M. (1987). The origin of Samoa: New evidence from Sr, Nd, and Pb isotopes. *Earth and Planetary Science Letters*, *81*(2–3), 151–162. https://doi.org/10.1016/0012-821X(87)90152-X

Yang, Z. F., & Zhou, J. H. (2013). Can we identify source lithology of basalt? *Scientific Reports*, *3*(1), 1856. https://doi.org/10.1038/srep01856

Yilmaz, Y., Saroglu, F., & Güner, Y. (1987). Initiation of the neomagmatism in East Anatolia. *Tectonophysics*, *134*(1–3), 177–199. https://doi.org/10.1016/0040-1951(87)90256-3

10.1029/2024GC011444

Zindler, A., & Hart, S. R. (1986). Chemical geodynamics. *Annual Review of Earth and Planetary Sciences*, *14*(1), 493–571. https://doi.org/10.1146/annurev.earth.14.1.493

Zor, E. (2008). Tomographic evidence of slab detachment beneath eastern Turkey and the Caucasus. *Geophysical Journal International*, *175*(3), 1273–1282. https://doi.org/10.1111/j.1365-246X.2008.03946.x

Zor, E., Sandvol, E., Gürbüz, C., Türkelli, N., Seber, D., & Barazangi, M. (2003). The crustal structure of the East Anatolian plateau (Turkey) from receiver functions. *Geophysical Research Letters*, *30*(24), 2–5. https://doi.org/10.1029/2003GL018192

References From the Supporting Information

Le Bas, M. J., Maitre, R. W. L., Streckeisen, A., & Zanettin, B. (1986). A chemical classification of volcanic rocks based on the total alkali-silica diagram. *Journal of Petrology*, *27*(3), 745–750. https://doi.org/10.1093/petrology/27.3.745

Irvine, T. N., & Baragar, W. R. A. (1971). A guide to the chemical classification of the common volcanic rocks. *Canadian Journal of Earth Sciences*, *8*(5), 523–548. https://doi.org/10.1139/e71-055

Miyashiro, A. (1974). Volcanic rock series in island arcs and active continental margins. *American Journal of Science*, *274*(4), 321–355. https://doi.org/10.2475/ajs.274.4.321

Miyashiro, A. (1978). Nature of alkalic volcanic rock series. *Contributions to Mineralogy and Petrology*, *66*(1), 91–104. https://doi.org/10.1007/BF00376089

Sun, S. S., & McDonough, W. F. (1989). Chemical and isotopic systematics of oceanic basalts: Implications for mantle composition and processes. *Geological Society Special Publication*, *42*(1), 313–345. https://doi.org/10.1144/GSL.SP.1989.042.01.19